How interactions between tropical depressions and western disturbances affect heavy precipitation in South Asia

How Interactions between Tropical Depressions and Western Disturbances Affect Heavy Precipitation in South Asia

KIERAN M. R. HUNT,[a,b] ANDREW G. TURNER,[a,b] AND REINHARD K. H. SCHIEMANN[a,b]

[a] *National Centre for Atmospheric Science, University of Reading, Reading, United Kingdom*
[b] *Department of Meteorology, University of Reading, Reading, United Kingdom*

(Manuscript received 9 November 2020, in final form 22 March 2021)

ABSTRACT: Interactions over South Asia between tropical depressions (TDs) and extratropical storms known as western disturbances (WDs) are known to cause extreme precipitation events, including those responsible for the 2013 floods over northern India. In this study, existing databases of WD and TD tracks are used to identify potential WD–TD interactions from 1979 to 2015; these are filtered according to proximity and intensity, leaving 59 cases that form the basis of this paper. Synoptic charts, vorticity budgets, and moisture trajectory analyses are employed to identify and elucidate common interaction types among these cases. Two broad families of interaction emerge. First, a dynamical coupling of the WD and TD, whereby either the upper- and lower-level vortices superpose (a *vortex merger*), or the TD is intensified as it passes into the entrance region of a jet streak associated with the WD (a *jet-streak excitation*). Second, a moisture exchange between the WD and TD, whereby either anomalous moisture is advected from the TD to the WD, resulting in anomalous precipitation near the WD (a *TD-to-WD moisture exchange*), or anomalous moisture is advected from the WD to the TD (a *WD-to-TD moisture exchange*). Interactions are most common in the post-monsoon period as the subtropical jet, which brings WDs to the subcontinent, returns south; there is a smaller peak in May and June, driven by monsoon onset vortices. Precipitation is heaviest in dynamically coupled interactions, particularly jet-streak excitations. Criteria for automated identification of interaction types are proposed, and schematics for each type are presented to highlight key mechanisms.

KEYWORDS: Extratropical cyclones; Extreme events; Monsoons; Rainfall; Synoptic-scale processes

1. Introduction

The devastating 2013 north India floods were caused by unusually heavy rainfall after a trough in the upper-tropospheric westerlies interacted with a strong monsoon low pressure system (Mishra 2015; Chevuturi and Dimri 2016). Such interactions between these extratropical systems—known commonly as western disturbances—and tropical depressions, whether or not embedded in the summer monsoon, have the potential to cause extreme precipitation for several reasons. First, the region is rich in steep, complex orography resulting in areas of very large climatological precipitation; second, tropical systems that cannot necessarily reach these regions might be able to provide moisture to the extratropical systems that do pass over such areas.

Western disturbances (WDs; also known as *westerly troughs*) are most common during the winter months (Lang and Barros 2004; Madhura et al. 2015; Hunt et al. 2018a) when the subtropical westerly jet in which they are embedded is farthest south, over the Indian subcontinent (Schiemann et al. 2009). These WDs occur 5–10 times per month in winter, are largely confined to the middle and upper troposphere (e.g., Singh and Agnihotri 1977; Roy and Roy Bhowmik 2005; Dimri and Chevuturi 2014; Cannon et al. 2016) and are extratropical (i.e., frontal and baroclinic) in nature (Pisharoty and Desai 1956; Rao and Rao 1971; Singh and Agnihotri 1977). WDs are responsible for the majority of winter precipitation over Pakistan, north India, and Nepal (Hunt et al. 2019b; Midhuna et al. 2020), especially over the western Himalaya (Palazzi et al. 2013), and for almost all extreme precipitation events during winter in north India and Pakistan, primarily drawing their moisture from the Arabian Sea (Hunt et al. 2018b).

Tropical depressions (TDs) occur over South Asia in two varieties, depending on the large-scale environment and season. During the summer monsoon, when vertical wind shear is extremely large, TDs cannot fully develop into tropical cyclones (e.g., Emanuel et al. 2004), instead becoming larger-scale monsoon low pressure systems (Sikka 1977). These low pressure systems occur 10–15 times per monsoon season and are responsible for over half of the rainfall in the monsoon core zone (Hurley and Boos 2015; Hunt and Fletcher 2019) as well as extreme rainfall events across north (e.g., Hunt et al. 2018b; Dutta et al. 2019), central (e.g., Rao 2001; Pai et al. 2015), and south (e.g., Tomar 2012; Hunt and Menon 2019) India. Outside the monsoon, in the absence of the severe vertical wind shear it brings, TDs are free to develop into tropical storms and

Denotes content that is immediately available upon publication as open access.

Supplemental information related to this paper is available at the Journals Online website: https://doi.org/10.1175/MWR-D-20.0373.s1.

Corresponding author: Kieran M. R. Hunt, k.m.r.hunt@reading.ac.uk

DOI: 10.1175/MWR-D-20-0373.1

tropical cyclones. The strongest of these, known in India as cyclonic storms (>17.5 m s^{-1} sustained wind speed) and severe cyclonic storms (>24.7 m s^{-1} sustained wind speed) occur on average three to four and one to two times per year, respectively (Singh et al. 2001), and can cause catastrophic rainfall in coastal regions of India and Bangladesh (e.g., Ali and Chowdhury 1997; Saha 2015; Akilan et al. 2017). A brief note on nomenclature: in this paper we use *tropical depression* to refer to all systems reaching at least tropical depression status, including monsoon low pressure systems, monsoon depressions, tropical storms, and tropical cyclones.

a. Interactions between tropical depressions and western disturbances

Interactions between western disturbances and tropical/monsoonal air masses have been the subject of a number of studies. Early on, it was theorized that TDs south of the Equator could affect the precipitation efficiency of WDs through interaction with the trade winds (Malurkar 1947). Pisharoty and Desai (1956) found that clusters of WDs around the Tibetan Plateau often preceded a break in the monsoon; such breaks were caused by low pressure associated with WDs steering the monsoonal westerlies poleward, causing deficient rain in the monsoon core zone and a surplus along the Himalayan foothills (Ramaswamy 1976; Yasunari 1986). Similarly, it has been shown that when the monsoon trough is situated anomalously far north, passing WDs can directly induce moist southerlies to reach the foothills (Kalsi 1980), and that WDs can create regions of high baroclinicity, and hence the potential for heavy precipitation, within the monsoon trough itself (Singh and Chand 2015).

Some work has also explored the more direct relationship between WDs and TDs, often noting that passing WDs appear to support cyclogenesis in the Bay of Bengal (Sen 1959; Prasad and Krishna Rao 1974), or strengthen existing depressions (George and Datta 1965; Kalsi and Jain 1989). George and Datta (1965) found, however, that quasigeostrophic analysis was not possible in the vicinity of the Himalayas due to contributions from mechanical forcing and friction, though it was later hypothesized that the intensification is caused by a decrease in altitude of the WD vorticity (Kalsi and Jain 1989). Srinivasan et al. (1973) found a correlation between WD presence and thunderstorm frequency over Bangladesh, though their study was confined to derechos. WDs can also cause depressions or tropical cyclones in the Bay of Bengal to recurve and head northward or northeastward (Joseph 1978, 1981; Rasul et al. 2005; Sikka 2006a).

Kalsi and Halder (1992), summarizing Rao (1976), identified four ways in which WDs interact with the tropics: (i) intensification or initiation of TDs; (ii) enhancing precipitation within existing TDs; (iii) causing TDs to recurve northward; and (iv) triggering breaks in the monsoon. Kalsi and Halder (1992) developed this thinking further, using satellite data to examine seven case studies of WD–TD interaction. They found that such interactions could occur before, during, or after the monsoon, often leading to distortions in the TD cloud field, and that they were often associated with heavy precipitation. Further, they confirmed in some cases that immature depressions could be intensified by WDs, but they could also be weakened by vertical wind shear associated with WDs. In one case, they found that outflow from a tropical cyclone affected a WD.

Interest in WD–TD interactions surged after the 2013 Uttarakhand/north India floods; a number of authors described the cause as being a merger of a monsoon low pressure system and a western disturbance, noting that it was preceded by the former redirecting moist southerlies into the affected region (Singh and Chand 2015; Joseph et al. 2015; Ranalkar et al. 2016; Vellore et al. 2016; Houze et al. 2017).

b. Interactions between tropical cyclones and upper-tropospheric troughs

There are some important dynamical similarities between WD–TD interactions and the interactions of tropical cyclones (TCs) and upper-tropospheric troughs (UTTs), which have been the focus of a much wider range of studies, typically focused on the United States. However, there are three principal differences, particularly for monsoonal (or otherwise non-TC) TDs. (i) WD–TD interactions almost invariably happen over land, and often near steep orography, whereas most TC–UTT interactions occur over the ocean. (ii) The mechanisms behind TC and TD growth differ—TCs are thought to grow either through wind–evaporation feedback (Emanuel 1986) or through vortical hot towers (Montgomery et al. 2009), whereas TDs (in particular monsoonal TDs) are thought to grow through interactions between moist convection and the monsoonal mean state—including both horizontal and vertical shear and the distribution of moist static energy (Diaz and Boos 2019, 2021; Adames 2021). (iii) Wind shear is detrimental for TC growth (e.g., DeMaria 1996) as it ventilates the TC core with low entropy air, but is either beneficial (see above) or insignificantly detrimental for TD growth (Moorthi and Arakawa 1985; Rao et al. 2004; Ditchek et al. 2016). Although these differences must be borne in mind when placing the work of this paper into context, much insight into the processes behind WD–TD interactions can be gained from thorough analysis of the TC–UTT interaction literature.

The first comprehensive assessment of TC–UTT interactions was undertaken by Sadler (1976), who developed a conceptual model based on three case studies. He noted three important factors that made these interactions favorable for developing TCs: decreased vertical wind shear, increased divergence aloft, and channeling of the TC outflow into large-scale westerlies. Following this, a number of mechanisms by which a UTT could lead to TC intensification have been proposed. First, some authors found that the azimuthal eddy flux convergence of angular momentum induced by the UTT interacting with the TC outflow could enhance the secondary circulation of the TC (Pfeffer and Challa 1981; Molinari and Vollaro 1989; Hanley et al. 2001). However, this mechanism is unlikely to be important in TD–WD interactions because TDs almost always lack eyewalls. Second, TC outflow can be directly enhanced by the secondary circulation associated with an accelerating westerly jet upshear of the UTT, which reduces inertial stability aloft (Shi et al. 1990, 1997; Rios-Berrios et al. 2016; Komaromi and Doyle 2018). A variant of this was also

proposed by Rodgers et al. (1991), who found that when the TC outflow was channeled into the westerly jet, intense convective outbreaks could be initiated and sustained in mature TCs below. This mechanism is possible for TD–WD interactions over South Asia, given that WDs propagate along the subtropical westerly jet. Third, authors have considered the constructive way in which the positive PV anomalies of the UTT and TC can interact when they are superposed. Some have proposed that this occurs directly through quasigeostrophic forcing (Molinari et al. 1995; Bosart et al. 2000; Bracken and Bosart 2000; Fischer et al. 2017, and as a secondary mechanism by Galarneau et al. 2015), arguing that the PV cutoff low that forms the UTT is sufficiently small in scale to generate significant QG ascent through the differential vorticity advection term. Others have proposed that the upper-level anomalous PV is advected directly into the TC (Leroux et al. 2016), or that it is redistributed there by internal diabatic heating (Molinari et al. 1998; Hanley et al. 2001; Fischer et al. 2017). This mechanism is also possible for WD–TD interactions, as WDs have a PV maximum in the upper troposphere and TDs have a PV maximum in the lower troposphere, allowing for superposition.

Despite these proposed intensification mechanisms, it has long been known that some UTT interactions can weaken or terminate TCs (Lewis and Jorgensen 1978; Zehr 1992). Subsequent authors found that the relative location (DeMaria et al. 1993; Komaromi and Doyle 2018), size (Molinari et al. 1998; Fischer et al. 2017), and strength (Molinari et al. 1998) of the UTT determine whether the resulting vertical wind shear is damaging to the TC or not. WDs do not vary appreciably in size, but their intensity can vary over an order of magnitude (Hunt et al. 2018a), which, along with changes in relative position, could significantly affect the nature of their interactions with TDs.

Of particular interest to this work are those studies that have sought to classify interactions according to their composite dynamics. Hanley et al. (2001) examined potential UTT interactions among all named North Atlantic TCs from 1985 to 1996 using an eddy momentum flux convergence framework. They reduced these interactions into four categories: favorable and unfavorable superposition (if the TC intensified or weakened within 400 km of the UTT PV maximum), and favorable and unfavorable distant interaction (TC between 400 and 100 km from UT PV maximum). They did not attempt to determine the cause of unfavorable superpositions due to a very small sample size, but ascertained that the difference between favorable and unfavorable distant interactions was typically excess wind shear in the latter caused by a strong UTT. These distant interactions were characterized by the TC passing into the jet entrance region downstream of the UTT, as discussed above. Fischer et al. (2017) classified TC–UTT interactions by TC intensification rate. They found that the most rapid intensification rates were associated with QG-forced ascent in upshear quadrants of the TC, driven—in agreement with earlier studies—by differential vorticity advection. The weakest (i.e., neutral) intensification rates occurred when the UTT and TC where very close, with the jet over the developing TC resulting in unfavorable wind shear. Fischer et al. (2019) then used a *k*-means approach to retrieve clusters of UTT features involved in rapid TC intensification. They identified three clusters, a ''cutoff'' UTT cluster, which they associated with the superposition interaction in Hanley et al. (2001), a ''northwest'' UTT cluster, which they associated with the distant interaction in Hanley et al. (2001), and a ''northeast'' UTT cluster. They found that among these, rapid intensification was most likely in the cutoff and northeast clusters, and preferred a short UTT wavelength, with a distance of 500–1000 km between the UTT and TC PV maxima.

c. *Summary*

Despite the work of Kalsi and Halder (1992) and studies on the 2013 north India floods, several issues remain unclear. Though databases of various flavors of TD have existed for some time [e.g., monsoon low pressure systems (Sikka 2006b), monsoon depressions (Mooley and Shukla 1989), and tropical cyclones (Gray 1985)], such a catalogue for WDs did not exist until fairly recently (Hunt et al. 2018a). As such, there has not yet been an attempt to describe the interactions between TDs and WDs in a climatological framework, meaning that we have a number of key unanswered questions:

- How frequently do interactions between WDs and TDs occur?
- Are there different types of interaction?
- How do WD–TD interactions affect precipitation, and how does this vary by interaction type?

In this study, we will discuss our data and methods in section 2. We will then detail different interaction types and their rainfall production mechanisms (section 3), and then look at broad interaction statistics such as location and seasonality (section 4). An outline for automatic identification of interaction types is presented in section 5. Finally, we discuss the implications of our work in section 6 and conclude in section 7.

2. Data and methodology

a. *Data*

The five datasets used in this study are described below.

For the atmospheric variables plotted in our synoptic charts, as well as for the fields needed for trajectory analysis, we use the European Centre for Medium-Range Weather Forecasts interim reanalysis (ERA-I; Dee et al. 2011). All fields are available at 6-hourly intervals with a horizontal resolution of T255 (~78 km at the equator), with the three-dimensional fields distributed over 37 vertical pressure levels spanning from the surface to 1 hPa. The dataset covers the period 1979–2019. Data are assimilated into the forecasting system from a variety of sources, including satellites, ships, buoys, radiosondes, aircraft, and scatterometers. ERA-I outputs derived purely from the model, for example precipitation and cloud cover, are not used in this study.

Precipitation data in this study come from the APHRODITE-2 project (Yatagai et al. 2012, 2017), which is based on gauge data, gridded using a kriging method to 0.25° × 0.25° at daily resolution. The dataset runs from 1951 to 2015. Over India, the rainfall amount recorded for a given day is the accumulation

from 0300 UTC (0830 LT) the previous day to 0300 UTC of the current day. This dataset was chosen for its longevity and resolution. Given we are not interested in rainfall over the ocean, satellite data were not needed. The sparse gauge network over the Himalayas and Hindu Kush (as well as the difficulties of measuring snowfall with gauges) means that precipitation data in this region have significant uncertainty.

To check the robustness of our results, we will also use precipitation data from the high-resolution Indian Monsoon Data Assimilation and Analysis (IMDAA) reanalysis (Ashrit et al. 2020). This reanalysis is available at an hourly sampling frequency from 1979–2018 over the South Asian region (15°S–45°N, 30°–120°E), at a spatial resolution of 12 km, and simulated precipitation well when verified against individual gauges (Ashrit et al. 2020).

We use the database of western disturbance tracks from Hunt et al. (2018a) in this study. Using 6-hourly ERA-Interim data, they tracked WDs by computing the mean relative vorticity in the 450–300-hPa layer, and then performed a spectral truncation at T63 to filter out short-wavelength noise. They then identified positive-definite vorticity regions within this field and determined the centroid location for each one. These centroids were then linked in time, subject to constraints in distance and steering winds, to form candidate WD tracks. Finally, those candidate tracks that did not pass through South Asia (20°–36.5°N, 60°–80°E), have a lysis to the east of their genesis. Tracks that did not last at least 48 h were rejected. This catalogue is publicly available from the CEDA repository (Hunt et al. 2019a).

We use the database of tropical depression tracks from Hunt and Fletcher (2019) in this study. The core of the algorithm is identical to that used to develop the western disturbance catalogue above, except the input is the truncated 900–800-hPa relative vorticity field. There is no domain filtering at the end, but tracks shorter than 48 h are still rejected. This algorithm has been used, either for WDs or TDs, by a number of authors (e.g., Martin et al. 2019; Dong et al. 2020; Arulalan et al. 2020).

b. Proximity calculation and event selection

Using the western disturbance and tropical depression track databases outlined in section 2, we start by parsing them to identify common 6-hourly samples in which both a WD and TD are present over South Asia. Here, South Asia is defined as 10°–35°N, 60°–90°E, though as we will come to see, the following results are insensitive to this choice. This first step gives us several thousand timesteps (4952, spread over 1066 unique WD–TD pairs) over the common track database period (1979–2014) with ''interactions,'' the majority of which are far apart and/or very weak (Fig. 1), and thus unlikely to interact with each other. We therefore filter through two additional criteria: first, we require the centers of the WD and TD to pass within 2000 km of each other; second, we require that the geometric mean of the relative vorticities at the system centers (taken at 850 hPa for TDs, 350 hPa for WDs) is greater than $5 \times 10^{-5}\,s^{-1}$. These thresholds correspond closely to the median interaction distance and the upper quartile interaction intensity, and coincide with ranges presented in previous literature (Patla et al. 2009) for TC–UTT interactions. Together, these criteria ensure that both systems are well-developed, and that they pass within an influencing distance of each other. This additional filter leaves us with several hundred interaction time steps, which belong to a total of 59 interacting WD–TD pairs. The selection process is summarized in Fig. 1, which further demonstrates the complex life cycles of these interactions. In an additional five cases, the WD and TD tracks were inseparable and clearly indicated that the same system had been tracked by both algorithms. Such cases are not considered in this paper. We make no effort to differentiate between tropical cyclones and weaker TDs in this process; however, among the 59 cases compiled, only two TDs had tropical cyclone status at the time of the interaction.

All 59 cases were analyzed manually and individually. For each, synoptic charts showing precipitation, vorticity, moisture flux, upper and lower level winds, and vertical velocity were produced for all times when both a TD and WD were present as well as a day either side. Then, the synoptic and subsynoptic-scale processes responsible for heavy precipitation in the vicinity of either system were described, along with the overall circulation and any additional features of interest, such as regions of unusually high moisture flux or precipitation. Common types of interaction were then identified from this list of synopses, with each case being assigned to one, two, or in six cases, zero types. Those cases not assigned a type are deemed to be noninteracting for the purpose of this study. That does not mean that no interaction has taken place, only that the methods we have deployed were insufficient to detect its pathway. In the sections that follow, each of the major types of interaction identified will be explained and analyzed using selected case studies that best illuminate their most important characteristics.

Broadly speaking, there are potential three ways in which a WD and TD can interact: through a change in the dynamics, a change in the moisture flux, or a change in the thermodynamics (i.e., through static stability). As we will come to see, these can manifest in several different ways, and are not necessarily mutually exclusive.

3. Categories of interaction

a. Dynamical coupling

Here, we identify two distinct types of WD–TD interaction where the key mechanism depends on some modulation of the dynamical fields. The first of these is a vortex merger, where the two systems physically combine; the second, which we call a jet-streak excitation, involves the WD inducing a downstream jet streak whose entrance region constructively interferes with a TD, strengthening it.

1) VORTEX MERGING

Vortex mergers between WDs and TDs are possible in principle because they largely inhabit different regions of the troposphere: WDs tend to have a vorticity maximum around 400–300 hPa (Dimri and Chevuturi 2016; Hunt et al. 2018a) whereas TDs tend to have theirs at about 900–800 hPa (Godbole 1977; Hurley and Boos 2015; Hunt et al. 2016).

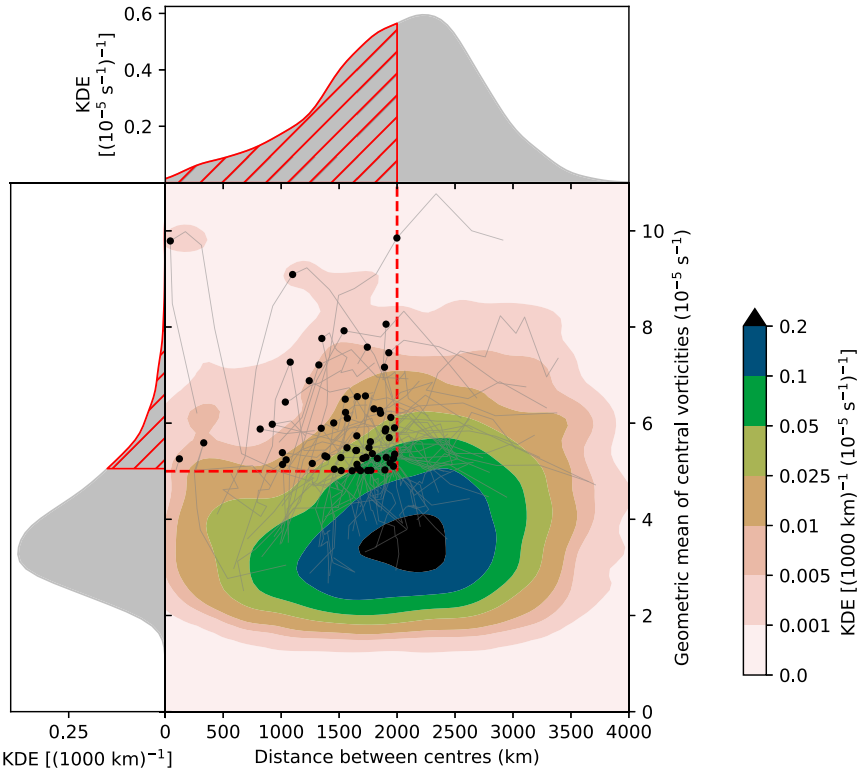

FIG. 1. Case studies shown in distance–intensity phase space. The selection thresholds [$\sqrt{\zeta_{350}(\mathrm{WD})\zeta_{850}(\mathrm{TD})} > 5 \times 10^{-5}\,\mathrm{s}^{-1}$ and separation distance of the TD and WD centers < 2000 km] are marked in red. Paths of the 59 cases meeting these criteria are given by gray lines, with exemplary points for each marked in black. Colored contours show a Gaussian kernel density estimate of the frequency of all interactions (on a time step, rather than event, basis). The univariate Gaussian kernel density estimates for (top) distance and (left) intensity.

Systems at similar altitudes (e.g., pairs of tropical cyclones) tend not to merge in this way (Fujiwhara 1921), but when they do the process is complex and typically involves the loss of convective organization of one of the systems (Lander and Holland 1993). Merger interactions are an analog to the "favorable superposition" interactions of Hanley et al. (2001) and the cutoff cluster of Fischer et al. (2019).

The first vortex merger case we consider occurred in November 1995 when a TD (mostly orange contours in Fig. 2) originating in the Bay of Bengal moved northwestward over the peninsula where it caused heavy precipitation over Nepal, Odisha, and Andhra Pradesh. Contemporaneously, a WD (magenta contours) moved southeastward across northern India. As the two systems approached each other, they both intensified (1800 UTC 9 November) before coalescing a day later (1800 UTC 10 November), causing 128 deaths and $46.3 million (USD) in damage over its duration (EM-DAT 2020).

To confirm whether these systems have actually merged, we need to look at the three-dimensional structure of relative vorticity. One way to do this is to project vortex filaments onto the surface by plotting a representative vorticity isoline ($2 \times 10^{-5}\,\mathrm{s}^{-1}$) at each vertical level (every 50 hPa in our case). Figure 2b shows how these filaments progress with time: initially the WD and TD are clearly separate top-heavy and bottom-heavy vortices, respectively. As the two approach (1800 UTC 9 November), some of the midtropospheric isolines start to combine while the upper and lower levels remain separated. This results in a vertical cross section that resembles an asymmetrical "H" shape. Eventually (1800 UTC 10 November), the system is described by a single isoline at each level, confirming a complete vortex merger. Figure 3 shows the development of the full vertical structure of relative vorticity and equivalent potential temperature during the merger. Aside from the features already mentioned, we note that a significant northwestward (i.e., along the line joining the two centers) tilt develops as the two systems merge (0000 UTC 10 November), remaining in the fully merged system (1200 UTC 10 November). Contours of equivalent potential temperature (black lines) show that a large frontal region develops as the highly baroclinic WD nears the deep convection of the TD (0600–1200 UTC 9 November). As this frontal region reaches the surface (1800 UTC 9 November to 0000 UTC 10 November), lower-tropospheric vorticity—associated with the TD—increases considerably in depth and magnitude. This suggests that slantwise convection may be resulting in vortex stretching in this region, which we will explore below. The final merged system (1200 UTC 10 November) has a complex thermal structure that retains baroclinicity in the

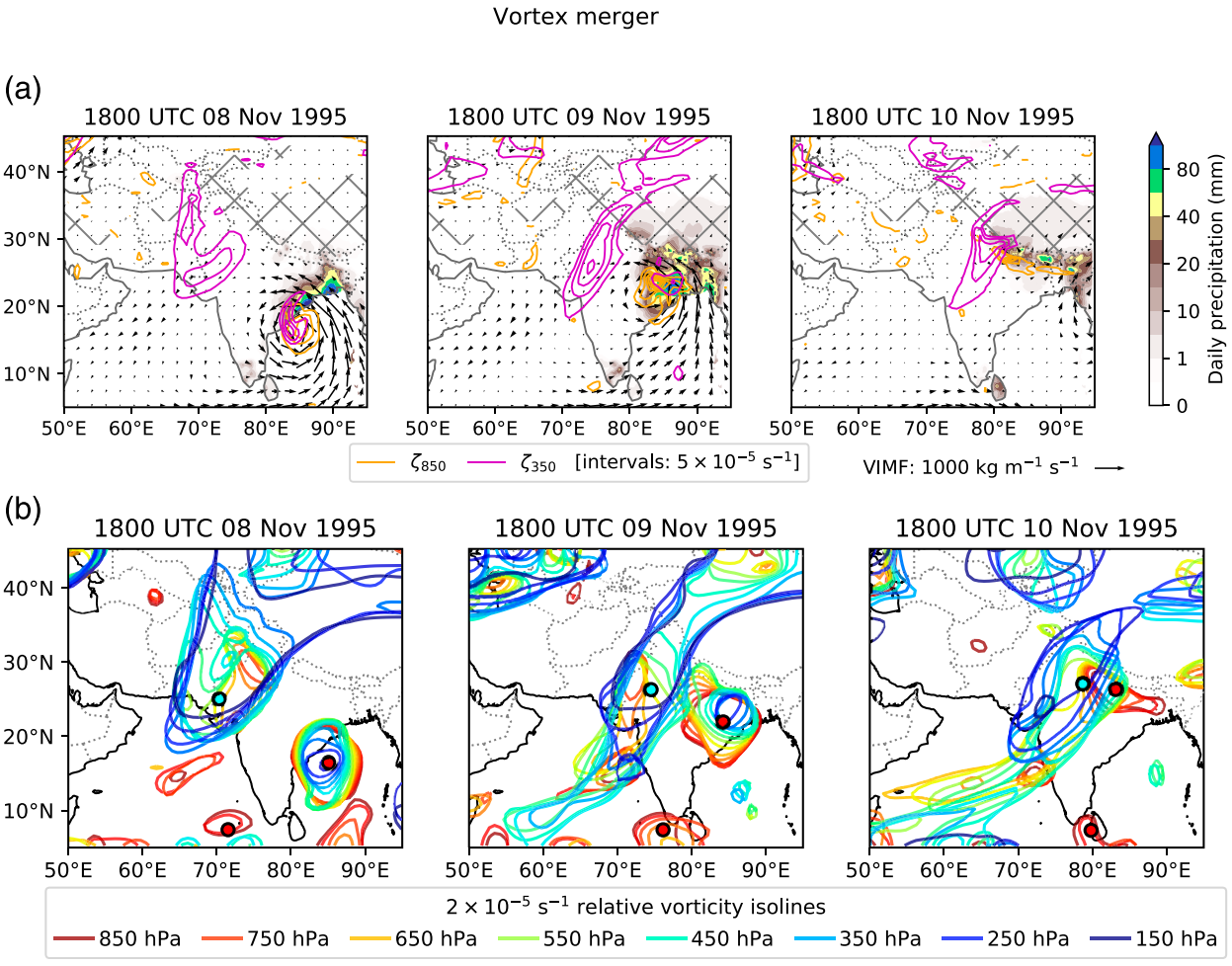

FIG. 2. Charts for 8–10 Nov 1995, showing a vortex merger. (a) Synoptic charts. Isolines, omitting zero, are shown for relative vorticity at multiples of 5×10^{-5} s^{-1} in orange (850 hPa) and magenta (350 hPa). Precipitation (solid color) is taken from APHRODITE and shows the 0300–0300 UTC daily total; arrows show the vertically integrated moisture flux. Coarse hatching indicates where surface pressure is below 850 hPa. (b) The structure of vorticity in the troposphere. For each pressure level from 850 to 150 hPa inclusive in 50 hPa intervals, the 2×10^{-5} s^{-1} relative vorticity isoline is plotted. Red circles mark the location of TDs, and cyan circles mark the location of the WD.

upper troposphere and a shallow vertical gradient in equivalent potential temperature in the lower troposphere, but also includes broad areas of relatively steep horizontal gradients, reflecting the mixing of tropical and subtropical air masses.

To complete this description of vortex mergers, we need to examine the vorticity tendency budget. This requires the selection of another case, November 1982, which occurs away from the Himalayan foothills where budget closure is difficult due to increased external body forces from the surface. In this case (Fig. 4), a tropical cyclone originated in the Arabian Sea, moving northeastward over Maharashtra and Gujarat. On making landfall, it weakened to depression intensity. At the same time, a WD, unusually far south, was tracking westward over the same area, resulting in a vortex merger and heavy precipitation over those states. There were an estimated 500 fatalities, 5 million displaced, and $625 million (USD) in damage (EM-DAT 2020) as a result.

There are a number of ways to write the vorticity tendency equation; here we choose to group terms by physical cause and neglect viscous diffusion and external forces, so

$$\underbrace{\frac{\partial \zeta}{\partial t}}_{\substack{\text{Eulerian rate}\\ \text{of change}}} = \underbrace{-\zeta \nabla_h \cdot \mathbf{u}_h}_{\substack{\text{Vortex}\\ \text{stretching}}} \underbrace{- \mathbf{u}_h \cdot \nabla \zeta}_{\substack{\text{Horizontal}\\ \text{advection}}} \underbrace{- \omega \frac{\partial \zeta}{\partial p}}_{\substack{\text{Vertical}\\ \text{advection}}} \underbrace{- \nabla_h \omega \times \frac{\partial \mathbf{u}}{\partial p}}_{\substack{\text{Vortex}\\ \text{tilting}}},$$

where ζ is the relative vorticity at a given pressure level, ω is the vertical velocity in pressure coordinates, $\mathbf{u}_h$ is the horizontal vector wind, and all other symbols have their usual meanings. The values of each of these terms for 0000 UTC 9 November 1982 (center panel of Fig. 4) at 800 hPa are shown in Fig. 5. This case is particularly useful because the TD vortex stalled as it made landfall, so contributions to the vorticity budget from storm translation—i.e., the contribution to $\partial\zeta/\partial t$ and $\mathbf{u} \cdot \nabla\zeta$ from movement of the vortex—were small.

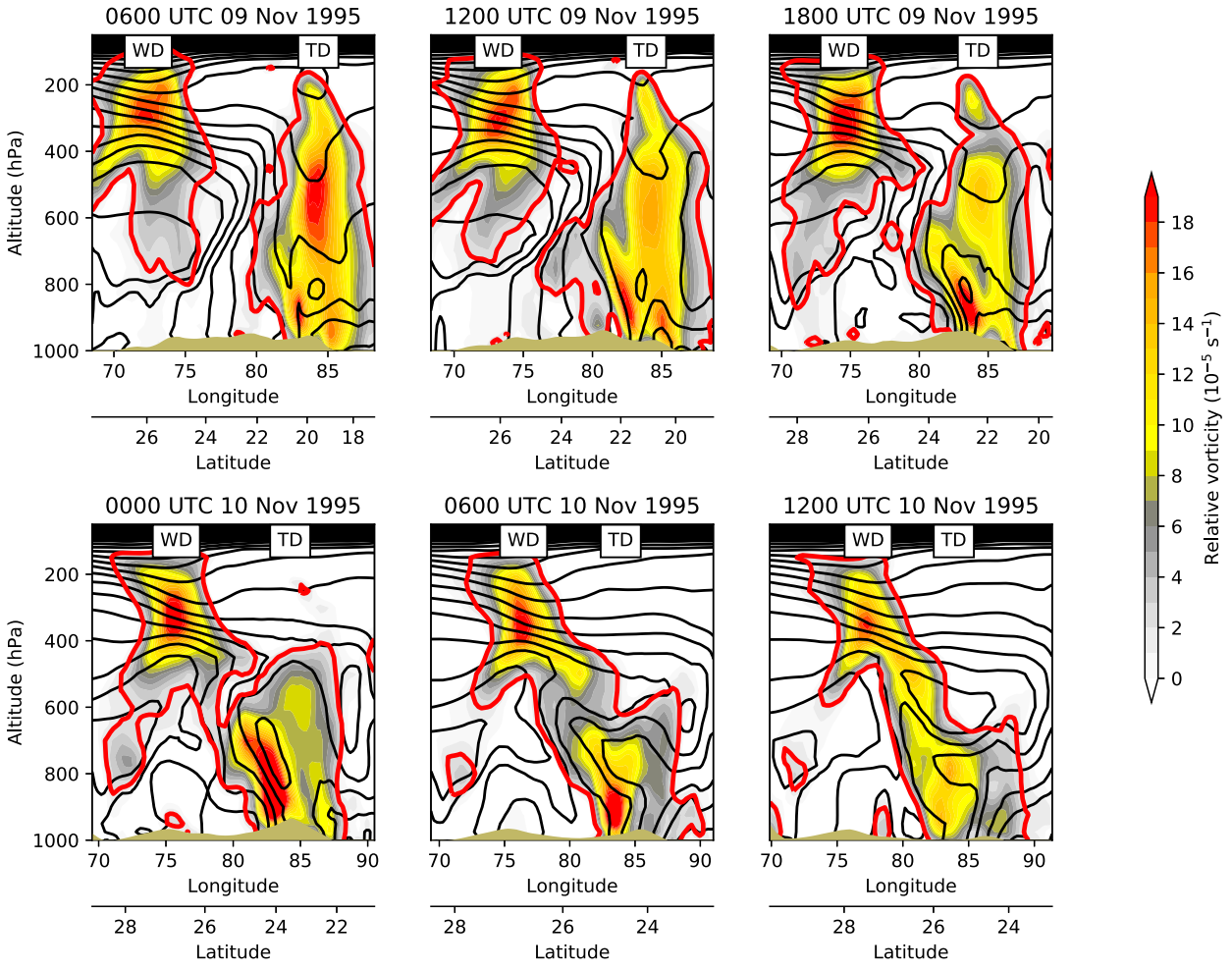

FIG. 3. Vertical cross sections of relative vorticity (filled contours) and equivalent potential temperature (black line contours; interval: 5 K) at 6-h intervals during the November 1995 vortex merger case. The horizontal axis is a geodesic of constant length, connecting the centers of the WD and the TD and is centered on their midpoint. The $2 \times 10^{-5}\,s^{-1}$ relative vorticity isoline is marked in red. Orography is filled in light brown.

The rate of change of vorticity (Fig. 5a) is calculated using a first-order differencing of the subsequent and current 6-hourly time steps in ERA-Interim, and shows both the slight northeastward progression of the vortex as well and its strengthening—as the positive tendency to the northeast is greater in magnitude than the negative tendency. Horizontal advection by steering winds (Fig. 5c) is largely cancelled out by the tilting term (Fig. 5e), with the residual tendency being slightly negative and to the east of the TD. Vertical advection (Fig. 5d) plays a minor role but at 800 hPa, at least, its contribution is dwarfed, along with the other terms, by vortex stretching (Fig. 5b). A brief caveat here: as Haynes and McIntyre (1987) point out, partitioning the vorticity equation in this way can lead to large noncancelling errors if there are uncertainties or inconsistencies in the input fields. However, given the relatively large scale of our analysis and the approximate budget closure in ERA-Interim, we do not believe that this significantly affects our results.

Other vortex merger cases (e.g., Fig. S1 in the online supplemental material) where the budget can be approximately closed show vortex stretching (b) to be the dominant term as well. Chen et al. (2005) showed that, at least for monsoonal TDs, lower-level vortex stretching is expected above regions of high precipitation due to latent heat release aloft, as did Adames and Ming (2018) and Clark et al. (2020) in GCM studies of varying complexity. While we do observe that here, and in other cases, the magnitude of the stretching term is several times higher during a merger interaction than for a standalone TD, implying that the interaction is responsible for some intensification of the TD through lower-level stretching. Budget analysis at 500 hPa (Fig. S2) shows that $\partial\zeta/\partial t$ is closely balanced by horizontal advection. This follows Boos et al. (2015) who found that steering of monsoonal TDs happens preferentially in the midtroposphere. At this level, the vertical advection term, caused by ascent, is both very large and collocated with the 850-hPa stretching, suggesting that the WD

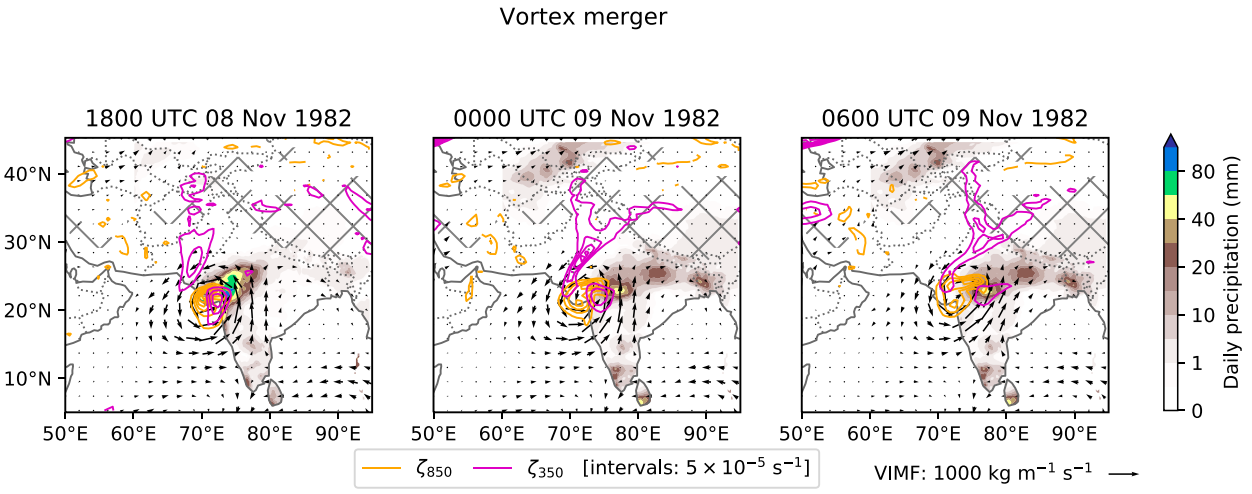

FIG. 4. Synoptic charts for 8–9 Nov 1982, showing a vortex merger. Isolines, omitting zero, are shown for relative vorticity at multiples of $5 \times 10^{-5}\,s^{-1}$ in orange (850 hPa) and magenta (350 hPa). Precipitation (solid color) is taken from APHRODITE and shows the 0300–0300 UTC daily total; arrows show the vertically integrated moisture flux. Coarse hatching indicates where surface pressure is below 850 hPa.

promotes intensification of the TD at lower levels by midtropospheric ascent leading to stretching. These results are generalizable to the other vortex merger cases identified by this study (see section 4). We note this contrasts with Kalsi and Jain (1989) who hypothesized that the intensification was caused by a decrease in altitude of the WD vorticity maximum.

2) JET-STREAK EXCITATION

The second type of dynamical coupling interaction occurs when a WD is associated with a downstream jet streak in the subtropical jet. Irrotational ageostrophic flow is associated with positive vorticity advection to the right (generally south or southeast, for the NH subtropical jet) of the jet-streak entrance, which is in turn associated with a region of ascent (e.g., Martin 2006, p. 214). A passing TD can interact with such regions, which are favorable for their development. We will hereafter refer to this type of interaction as a *jet-streak excitation*. Jet-streak excitation interactions are an analog to the ''favorable distant interactions'' of Hanley et al. (2001) and the northwest UTT cluster of Fischer et al. (2019).

Our exemplar jet-streak excitation case study occurred during September 1995 (Fig. 6) when a monsoonal TD initiated over central India and headed north, passing under a jet-streak entrance region that was associated with a WD over Afghanistan. Figure 6 highlights the structure of jets at 850 hPa (blue), 500 hPa (yellow), and 300 hPa (green) by plotting barbs for only the top quartile of wind speed at that level. The jet streak is clearly visible at 300 hPa, aligned toward the northeast with an entrance region broadly over Pakistan. The associated ascent region is highlighted by the gray contours indicating integrated vertical mass flux at about 30°N, 80°E, and for completeness, one can see the corresponding descent region to the left of the jet-streak entrance situated at about 40°N, 65°E. The TD (location given by red circle, full track—1200 UTC 1 September to 1800 UTC 4 September—by magenta line) passed into this ascent region and in doing so rapidly intensified and deposited heavy precipitation over the northern states of India, resulting in a flash flood in Bihar that killed nearly 1500 people (EM-DAT 2020). Inspection of synoptic charts from the preceding day verifies that the ascent region associated with the jet entrance is initially distinct from the depression and is not caused by its presence.

This intensification can be understood by looking at the evolution of the vertical structure of dynamic fields associated with the TD in Fig. 7. Here, we take vertical velocity, Q-vector convergence, and relative vorticity, averaging each over a circle of radius 2° centered on the TD. The TD was initially weak and shallow, with ascent confined to below 700 hPa. After initially spinning up on 1 September, the TD then weakened through 2 September. This is relatively common among land-forming depressions during the late monsoon, where the resources required to sustain a depression are typically limited (Baisya et al. 2017). From 3 September onward, Q-vector convergence, which indicates quasi-geostrophically forced ascent and creation of cyclonic vorticity below, steadily increased in the midtroposphere as the TD approaches the jet-streak entrance region. The increasing Q-vector divergence aloft is consistent with the structure expected from a jet-streak entrance (e.g., Martin 2006, p. 216). As the TD entered this region, its associated relative vorticity and vertical velocity increased significantly, resulting in a deepening of the ascent to over 300 hPa. While the vertical velocity and vorticity initially increased together, as one would expect, the former reached a maximum that was sustained for about 12 h longer. This was probably due either to latency from the initial intensification at lower levels or additional mechanical forcing from the Himalayan foothills. This pattern of Q-vector convergence mapping directly onto increases in vorticity and ascent was present in all other jet-streak

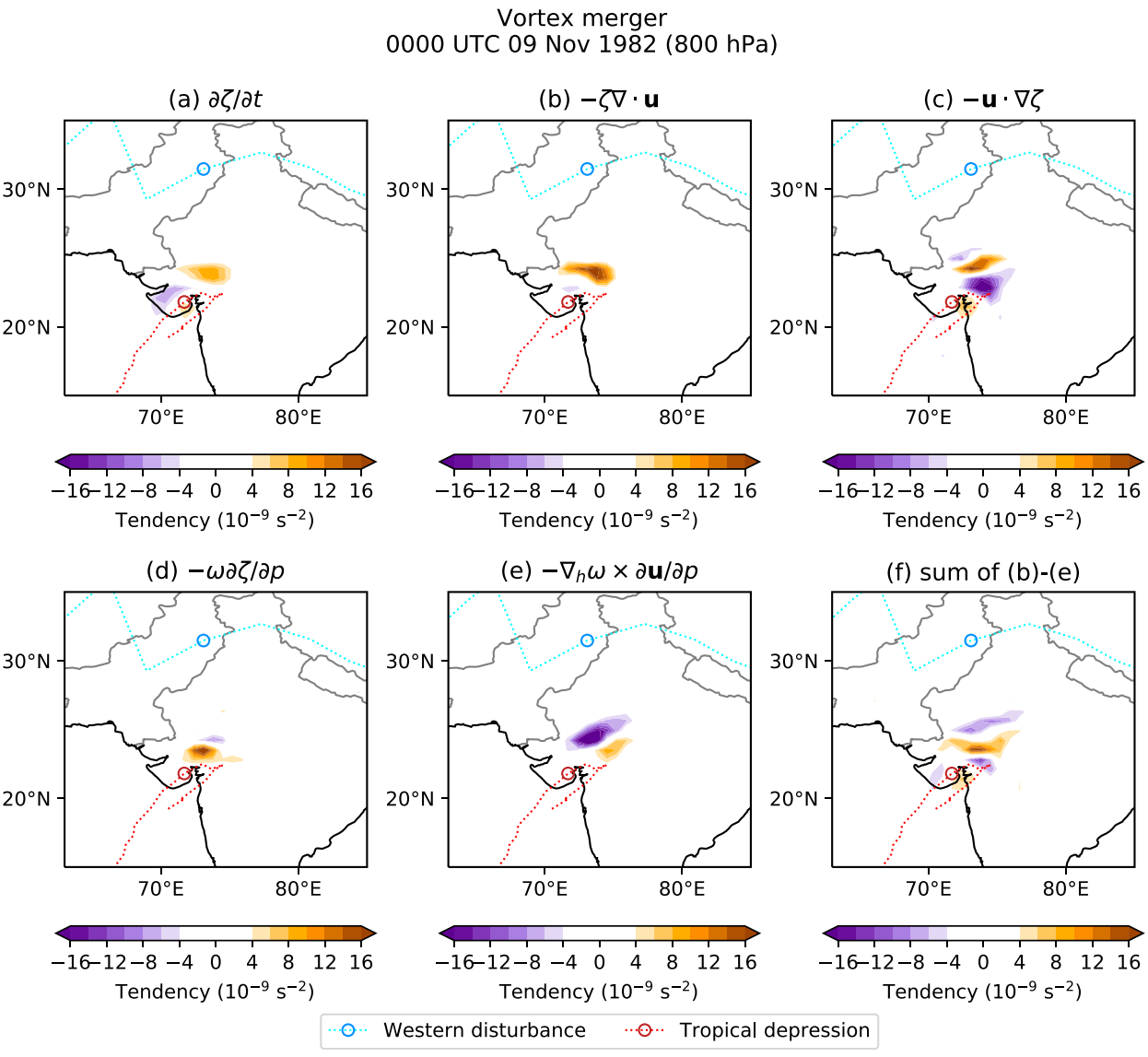

FIG. 5. Vorticity tendency budget at 800 hPa for 0000 UTC 9 Nov 1982. Tracks (dotted lines) and locations (circles) for the WD and TD are given in blue and red, respectively. (a) The Eulerian rate of change, (b) vortex stretching, (c) horizontal advection, (d) vertical advection, (e) vortex tilting, and (f) the sum of all tendency terms. The WD genesis was over the Mediterranean on 25 Oct 1982, and its lysis was over central China on 12 Nov 1982. The TD spun up over the Arabian Sea on 3 Nov 1982 and lasted until 11 Nov 1982.

excitation cases (examples shown in Figs. S3 and S4) examined during this study, as was the delayed deepening of the ascent.

b. *Moisture exchange*

Aside from coupling dynamically, WDs and TDs can also interact by exchanging moisture. In this section, we explore the mechanisms that commonly underlie this.

1) TD-TO-WD MOISTURE EXCHANGE

The next family of interactions are characterized by the transmission of moisture from one system to another. They do not necessarily couple dynamically as in the previous section, but instead provide or redirect moisture flux that amplifies the precipitation associated with one system or the other. The more common orientation is moisture flux gathered by the TD being sent northward or northwestward to be converted into precipitation by the WD. TD-to-WD moisture exchange interactions are dynamically similar to the predecessor rainfall events identified in Galarneau et al. (2010), wherein tropical cyclones provide deep tropical moisture to regions of quasi-geostrophically forced ascent associated with jet-streak entrances in the northern United States. However, WDs are not necessarily associated with jet streaks and the orography differs considerably between the two regions, so the forcing involved may differ considerably.

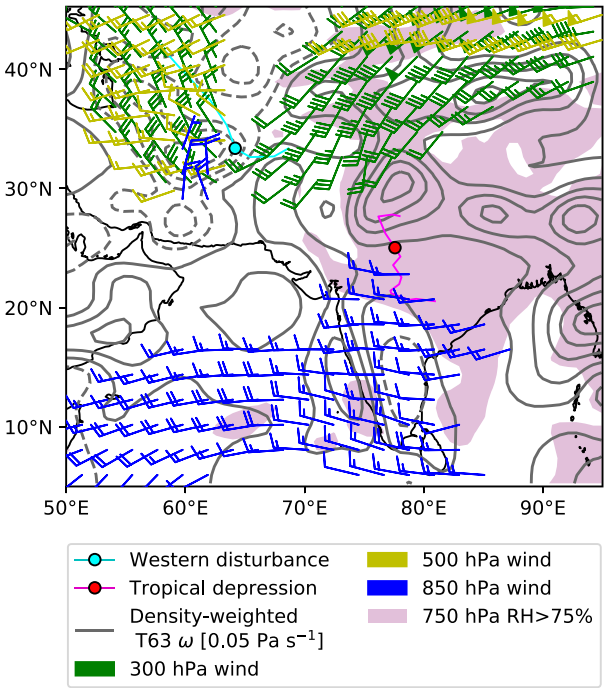

FIG. 6. Synoptic chart for 1800 UTC 3 Sep 1995 showing the top-quartile winds at 850 hPa (blue barbs), 500 hPa (yellow barbs), and 300 hPa (green barbs); tropospheric-mean vertical mass flux [given here as a density-weighted column-mean vertical velocity (ω); gray line contours, with solid for ascent and dashed for descent]; 750-hPa relative humidity (shaded purple where greater than 75%); and the locations of the WD (red marker) and TD (cyan marker).

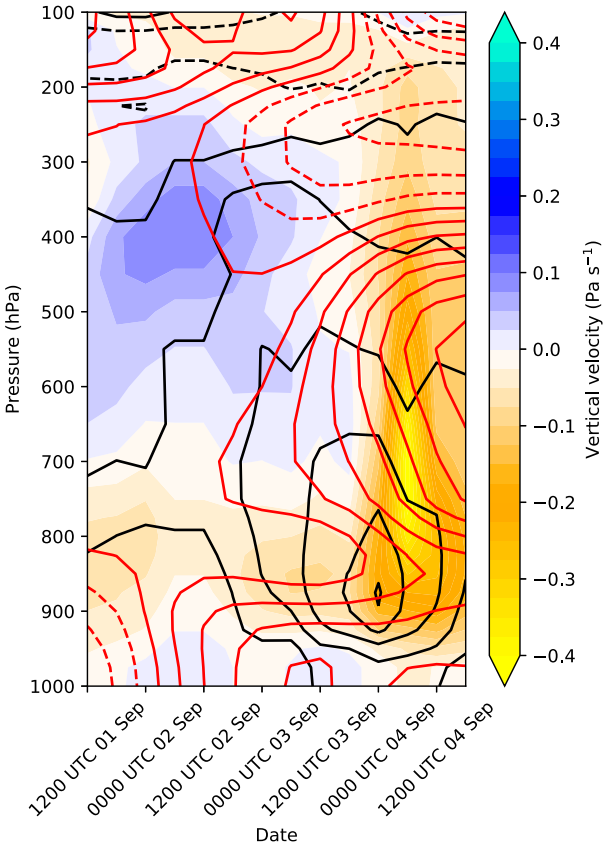

FIG. 7. Vertical structure of ω [solid contours], relative vorticity [black contours, interval: 2×10^{-5} s^{-1}, negative contours dashed], and Q-vector convergence [red contours, interval: 2.5×10^{-19} m s^{-1} kg^{-1}, negative contours dashed] for the TD shown in Fig. 6, involved in the jet-streak excitation that occurred in Sep 1995. These are taken as averages over a circle of radius 2° centered on that TD.

Perhaps the most illuminating, and certainly well-known, case of a TD-to-WD moisture exchange interaction is the Uttarakhand/north India floods of June 2013 (Fig. 8a), where a monsoonal TD originated in the Bay of Bengal and moved northwestward across the Gangetic Plain. It reached the vicinity of a strong WD that was subsequently associated with extremely heavy rainfall in north India, causing flooding and landslides that killed over 6000, displaced over 500 000, and caused $1.1 billion USD in damage (EM-DAT 2020). The synoptic charts show the TD was embedded in the monsoonal front, though it is unlikely to have been an onset vortex given that these usually originate in the Arabian Sea (Krishnamurti et al. 1981; Webster et al. 1998). The monsoonal moisture flux curves around the TD to the north, where the precipitation occurs. This is quite unusual for a monsoonal TD, whose precipitation tends to be located to the southwest of the center (Rajamani and Rao 1981; Hunt et al. 2016), and it is also clear from the synoptic charts that this WD is not organizing its own moisture—i.e., moisture in the vicinity of the WD has not been advected there by circulation associated with the WD itself. This is not necessarily unusual among WDs, but is notable here because it implies this WD would have caused very little precipitation without the presence of the nearby TD.

Figure 8b shows this interaction in the context of large-scale moisture flux convergence and ascent. The WD (cyan circles, note there are two because this system had several distinct vortical centers) has a local region of ascent associated with it, marked by the dense gray contours, that starts just to the south (0600 UTC 15 June) but eventually moves to the southeast (0600 UTC 17 June) as it intensifies. This ascent region quickly becomes collocated with the heaviest precipitation as the TD moisture flux passes into it. High values of vertically integrated moisture flux convergence (purple) show that the flux is being consumed in these areas. VIMFC appears to lag behind precipitation, but this is probably an artifact of the daily accumulation in APHRODITE.

Air parcel back-trajectories from regions of high specific humidity (Fig. 8c) allow us to consolidate this argument. Here, we release 100 equally spaced parcels from 800 hPa over a box (marked in red) containing the highest daily precipitation; these are then integrated backward for 3 days and colored by specific humidity to indicate potential sources of moisture for heavy rainfall events. We use the solver defined in Hunt et al. (2018b). We see that the trajectories are largely cyclonic, wrapping around the TD. This structure is also present at 500 hPa (Fig. S5) in the second and third initialization times,

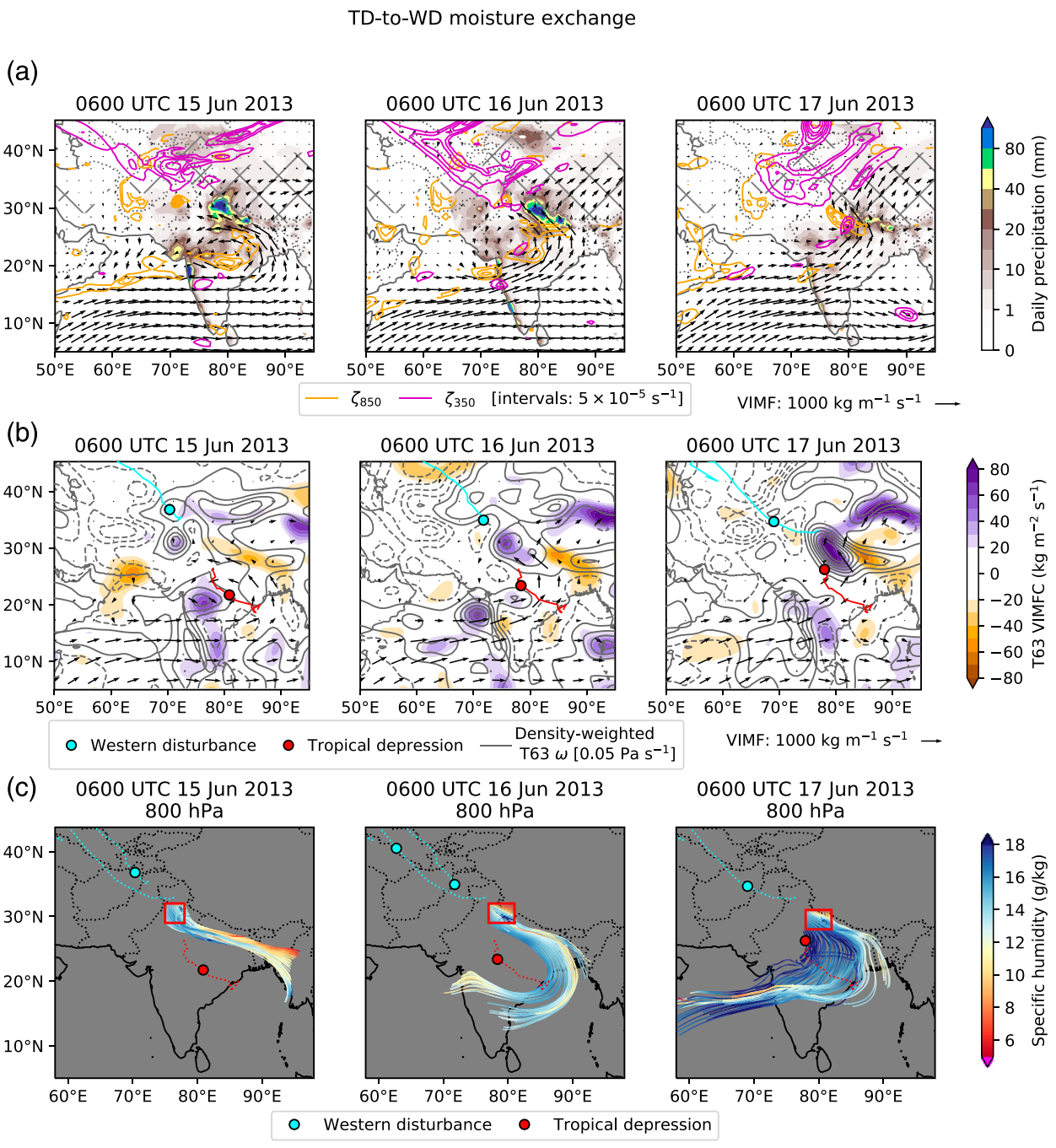

FIG. 8. Selected charts for 15–17 Jun 2013, showing a TD-to-WD moisture exchange interaction. Western disturbance tracks and locations are given in cyan; those for the TD are given in red. The TD lasted from 0000 UTC 12 Jun to 1800 UTC 16 Jun. The WD with which it interacted spun up over the Caspian Sea on 14 Jun and lasted until 1800 UTC 18 Jun. (a) Synoptic charts. Isolines, omitting zero, are shown for relative vorticity at multiples of $5 \times 10^{-5}\,s^{-1}$ in orange (850 hPa) and magenta (350 hPa). Precipitation (solid color) is taken from APHRODITE and shows the 0300–0300 UTC daily total; arrows show the vertically integrated moisture flux. Coarse hatching indicates where surface pressure is below 850 hPa. (b) Moisture-focused synoptic charts. Arrows show vertically integrated moisture flux. Colored contours show vertically integrated moisture flux convergence ($kg\,m^{-2}\,s^{-1}$), which has been spectrally truncated at T63 to aid illustration. Density-weighted vertically integrated vertical velocity is shown by gray contours (interval: $0.05\,Pa\,s^{-1}$; positive values dashed; zero contour in dark grey). Red and cyan lines mark the TD and WD tracks, respectively. (c) The 3-day back trajectories for air parcels originating over northern India at 0600 UTC on 15–17 Jun 2013, colored by specific humidity. For each time, 100 particles are released from 800 hPa, distributed evenly within a box (marked red) that contains the heaviest rainfall at that time. Red and cyan dotted lines mark the TD and WD tracks, respectively.

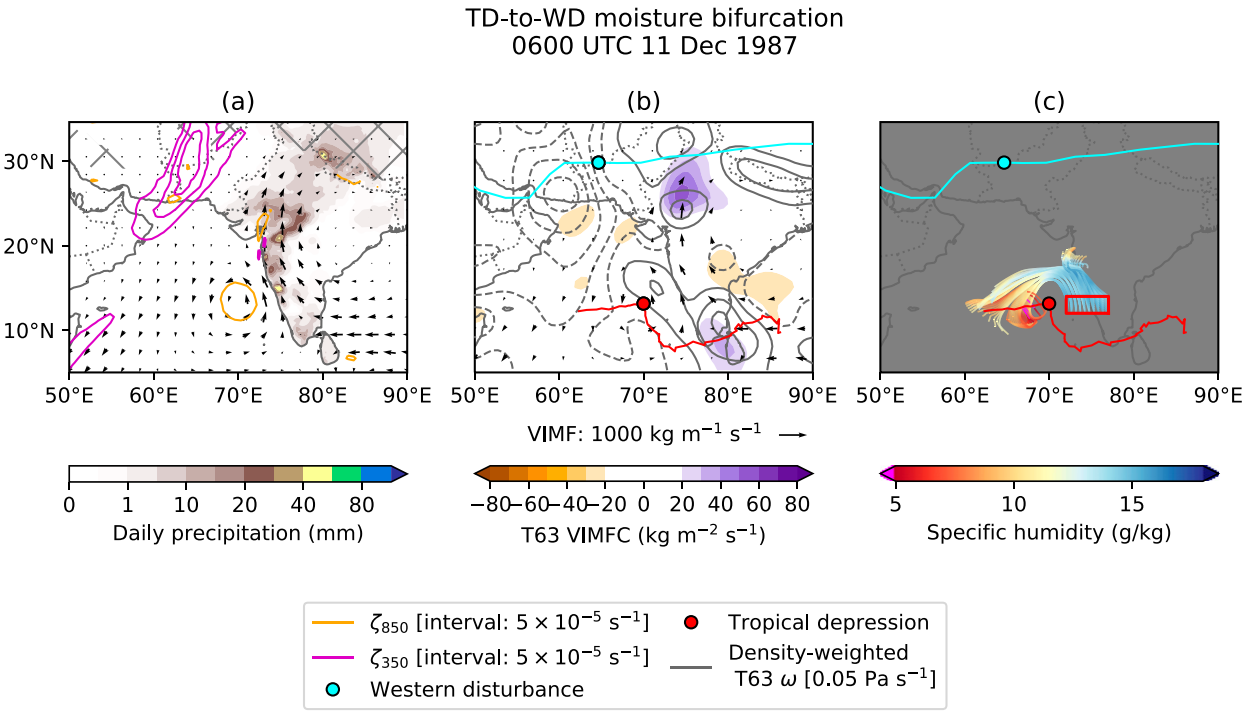

FIG. 9. A bifurcating TD-to-WD moisture exchange interaction at 0600 UTC 11 Dec 1987. (a) The synoptic situation, showing 0300–0300 UTC daily rainfall from APHRODITE, upper- and lower-level relative vorticity, and vertically integrated moisture flux. (b) The moisture-focused synoptic situation, showing vertically integrated moisture flux, its convergence, vertical mass flux, and the locations of the WD and TD. (c) The 3-day forward trajectories (colored by specific humidity; released at 750 hPa) from a region (marked by a red box) near the TD. The WD lasted from 5 Dec, when it spun up over the east Atlantic, to 13 Dec. The TD lasted from 30 Nov to 15 Dec. Red and cyan lines mark the TD and WD tracks, respectively.

indicating that almost all of the moisture present in the deep convection is brought in by circulation associated with the TD. This confirms that, even though the precipitation is closely related to the dynamics of the WD, the moisture is being provided almost wholly by the TD. Thus, the simultaneous presence of both systems enhanced the heavy rainfall preceding the floods.

(i) Bifurcation

TD-to-WD moisture exchange interactions appear to come in several different varieties, one of which is sufficiently distinct to merit discussion here. In most TD-to-WD moisture exchange interactions, the relative positioning of the two systems means that the moisture outflow from the TD passes directly into the WD; occasionally a very strong WD can induce the outflow from a nearby TD to change direction toward it, creating a separate branch of moisture flux, regardless of the relative position of the two systems. We will call this latter variant *bifurcation* for reasons that will shortly become clear.

Our case study of choice for TD-to-WD moisture bifurcation occurred in December 1987 (Fig. 9a) when a weak TD traversed the southern tip of peninsular India before turning north into the Arabian Sea; at the same time, a strong WD was moving eastward through Afghanistan and Pakistan. The strong ascent region associated with the WD (Fig. 9b), to its east, drives a region of significant lower-level convergence. This convergence splits the cyclonic moisture flux associated with the TD: as the circulation rotates from southerly to easterly along the southwest coast of India, one branch continues to head northward toward the WD. This southerly moisture flux is not climatological behavior since the mean lower-tropospheric winds over this region in December are northeasterly.

While it is difficult to prove that the convergence associated with the WD is related to the formation of the northward branch of moisture flux, we do have two additional pieces of evidence that support this claim. First, all other cases in which this bifurcation occurs have the split branch directed straight toward the WD convergence region – showing that the WD is responsible for its direction (though not necessarily its existence). Second, we can use forward trajectories (Fig. 9c) to show that moisture associated with the TD is physically separated into two branches, and that this is not, for example, a superposition of different phenomena on different layers. These trajectories, initialized at 0600 UTC 11 December, were computed in the same way as Fig. 8c except they were released at 750 hPa and integrated 3 days forward in time, rather than backward.

(ii) Preceding a merger

As we mentioned earlier, interaction types are not necessarily mutually exclusive. It is rare to see two interaction types occurring simultaneously, but not so uncommon for one to

follow another. Of these, by far the most common is a vortex merger preceded by an TD-to-WD moisture exchange interaction. An excellent example of this (Fig. S6), occurred between 13 and 17 October 1998, when a tropical storm spun up in the Arabian Sea and headed northeast over Gujarat. Before making landfall it provided a nearby WD with moisture flux resulting in widespread rainfall over northwest India. Several days later the two vortices merged over north India resulting in further precipitation over Himachal Pradesh and Uttarakhand. The extensive precipitation caused by this extended interaction resulted in about 250 fatalities (EM-DAT 2020), mostly fishermen in the Arabian Sea.

2) WD-TO-TD MOISTURE EXCHANGE

The alternative orientation for moisture exchange interactions involves transfer of moisture from the WD to the TD. This is typically less common than its opposite because, climatologically, TDs are embedded in warmer, moister tropical air masses, whereas WDs tend to sit in relatively drier, cooler extratropical air masses.

Our WD-to-TD moisture exchange interaction case study occurred in September 2003 (Fig. 10a), when a TD moved along the monsoon trough having started at the head of the Bay of Bengal; at the same time, a weak WD was moving southeastward through northern India. Heavy rains associated with the TD occurred in the state of Uttar Pradesh, resulting in fluvial flooding that killed 37 people. The synoptic charts show that initially the WD disrupts the monsoonal westerlies (0000 UTC 8 September), and eventually advects some moisture itself toward the TD (1200 UTC 9 September; see the small northwesterly flux in between the WD and TD centers).

The convergence/ascent charts (Fig. 10b) show that moisture from the WD was advected straight toward the region of ascent-driven moisture flux convergence to the west-northwest of the TD. This is near the expected location of ascent and maximum rainfall for monsoonal TDs, which is southwest of the center where it is driven by quasigeostrophic forcing arising from the interaction of the TD vortex and background monsoonal shear (Rajamani and Rao 1981; Boos et al. 2015). These figures suggest that, at least in this case, the moisture contribution from the WD was small but nonnegligible.

We can, to an extent, budget this contribution using moisture back-trajectories, as in Fig. 10c. Here, as in Fig. 8c, 100 evenly distributed (i.e., 10×10) parcels are released just above the boundary layer from a box containing the region with the highest daily rainfall at the times marked on the respective panels (0000 UTC 8 September, 1200 UTC 9 September, 0000 UTC 10 September). Initially (0000 UTC 8 September), as we observed in the synoptic charts, the WD does not seem to have provided any of its own moisture, rather briefly attracting the monsoonal westerlies. Much of the moisture associated with the heavy rainfall had already circulated at least once around the TD, rather than being provided directly by the westerlies encroaching into the northwest quadrant. Soon (1200 UTC 9 September through 0000 UTC 10 September), the WD develops as a moisture source in its own right, whereafter it is the source of about 15% of the trajectories reaching the heavy rainfall region (red box) 3 days later. Note that this more minor contribution stands in contrast to TD-to-WD moisture exchanges in which the TD provides almost all of the moisture to a WD. This contribution is largely consistent among all WD-to-TD moisture exchange interactions investigated, as is the preferential location of precipitation to the northwest of the TD center.

c. *Miscellaneous interactions*

1) SUCCESSIVE SYSTEMS

Both TDs and WDs can occur in rapid succession; indeed, TDs can occur simultaneously in the Arabian Sea and Bay of Bengal. Therefore, it is possible that some interactions could involve more than one of a given type of system. We observe several such cases (both two WDs with one TD and two TDs with one WD) in our dataset, one of which is shown in Fig. 11a. In this case, from October 1996, two TDs originated in the south of the Bay of Bengal within a few days of each other. The first moved westward over the south of the peninsula before stalling in the Arabian Sea, where it underwent a vortex merger (section 1) with a passing WD. The second moved due north toward the head of the bay, where it interacted via TD-to-WD moisture exchange with the same WD. As a result, there were heavy rainstorms over both the Arabian Sea and Bangladesh, the latter causing flooding of the Brahmaputra.

2) ONSET VORTICES

Onset vortices are an idiosyncratic feature of the Indian monsoon. As the monsoon advances northward across the subcontinent, the front that divides the strong monsoonal westerlies and weak, dry premonsoonal northwesterlies is rich in cyclonic shear and exists in an environment with regions of very large latent heat flux. As a result, TDs often spin up along this front, typically in the Arabian Sea (Krishnamurti et al. 1981). These are of particular interest because they occur while the subtropical jet is still fairly far south (it usually retreats northward during the monsoon, Schiemann et al. 2009), and thus are still supplying WDs to the subcontinent – providing ample chances for WD–TD interactions. Four of the 59 interactions investigated in this study directly involved an onset vortex, (e.g., Fig. 11b). In this June 2004 case, there are two onset vortex TDs, one in each basin. The Arabian Sea TD interacted via WD-to-TD moisture exchange with a passing weak WD resulting in very heavy oceanic precipitation southwest of the TD center. The TD in the Bay of Bengal did not interact with the WD. Interactions involving onset vortices are potentially dangerous because they can provide very heavy rainfall to arid premonsoonal areas of north India, though not in this case.

3) NO INTERACTION

As we saw in the previous case, it is possible for two systems to be reasonably strong and close to each other, but not interact. There were six such examples among our 59 cases, though given the manual nature of our determination of interaction types, they may well be interacting in a way not identified in this study. Figure 11c shows an example case, from October 1998. A TD initialized in the south of the Bay of

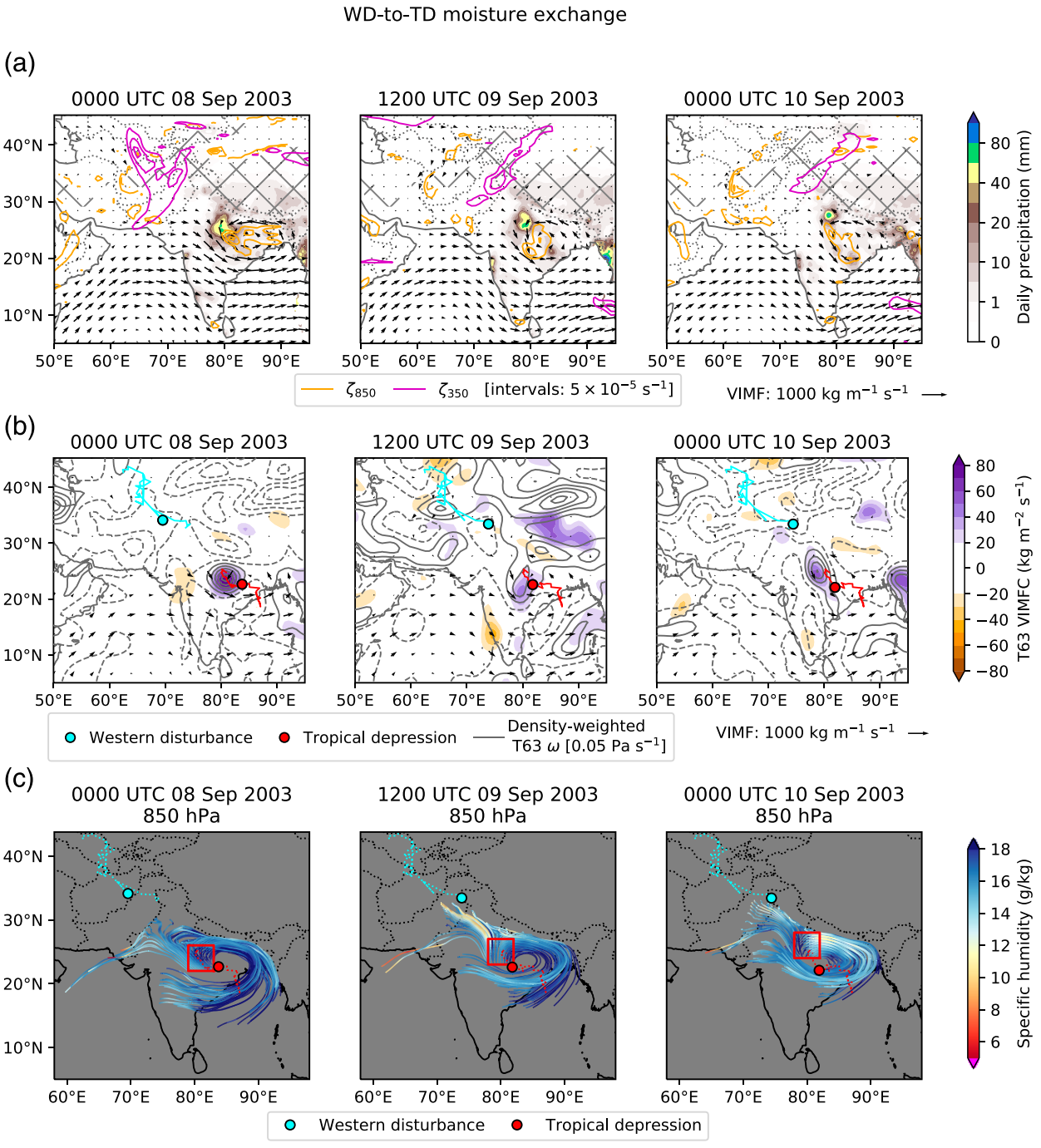

FIG. 10. Selected charts for 8–10 Sep 2003, showing a WD-to-TD moisture exchange. WD tracks and locations are given in cyan; those for the TD are given in red. The WD lasted from 1800 UTC 31 Aug to 0600 UTC 10 Sep. The TD lasted from 0600 UTC 4 Sep to 0600 UTC 12 Sep. (a) Synoptic charts. Isolines, omitting zero, are shown for relative vorticity at multiples of $5 \times 10^{-5}\,s^{-1}$ in orange (850 hPa) and magenta (350 hPa). Precipitation (solid color) is taken from APHRODITE and shows the 0300–0300 UTC daily total; arrows show the vertically integrated moisture flux. Coarse hatching indicates where surface pressure is below 850 hPa. (b) Moisture-focused synoptic charts. Arrows show vertically integrated moisture flux. Colored contours show vertically integrated moisture flux convergence ($kg\,m^{-2}\,s^{-1}$), which has been spectrally truncated at T63 to aid illustration. Density-weighted vertically integrated vertical velocity is shown by gray contours (interval: $0.05\,Pa\,s^{-1}$; positive values dashed; zero contour in dark gray). WD tracks and locations are given in cyan; those for the TD are given in red. (c) The 3-day back trajectories for air parcels originating over northern India at 0600 UTC 8–10 Sep 2003, colored by specific humidity. For each time, 100 particles are released from 850 hPa, distributed evenly within a box (marked red) that contains the heaviest rainfall at that time. Red and cyan dotted lines mark the TD and WD tracks, respectively.

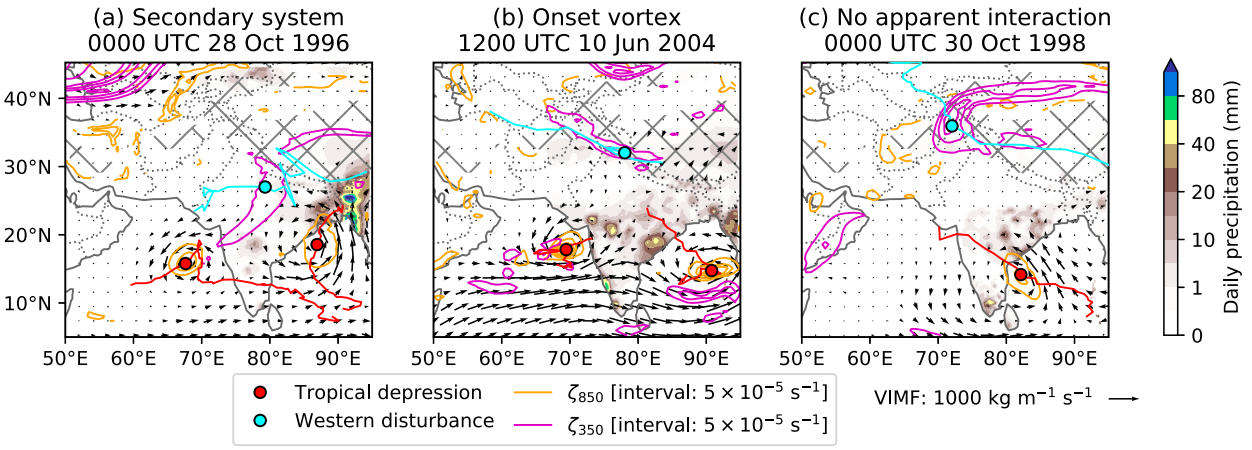

FIG. 11. Synoptic charts for selected interaction contexts showing (a) the involvement of a secondary TD; (b) monsoon onset vortices, which typically encroach on the peninsula in early June; and (c) the apparent lack of an interaction altogether, despite the presence of both a WD and a TD. As in previous figures, isolines of 850- and 350-hPa relative vorticity are shown in orange and magenta, respectively; locations and tracks of TDs and WDs are given in red and cyan, respectively; solid contours show daily rainfall; and arrows show vertically integrated moisture flux.

Bengal moved northwestward over the peninsula at the same time a strong WD passed through northern India. There was no exchange of moisture, nor any dynamical interaction, and the TD deposited a moderate amount of rainfall along the southeast Indian coast. It is not yet clear why this pair did not interact, when quite similar pairs have undergone TD-to-WD moisture exchange. Synoptic charts for the full timeline of this noninteracting case are given in Fig. S7.

4) SATELLITE EVENTS

In June 1983 (Fig. S8), an onset vortex that developed into a TD in the Arabian Sea interacted with a WD over north India in a way not observed in any of the other 58 cases. Both systems contributed moisture to the advancing monsoon westerlies, which, on impinging upon orography in northeast India several thousand kilometers away, caused heavy precipitation. We cannot generalize from a single case; however, this lends evidence to the capacity for WDs and TDs to interact simultaneously with a strong background flow resulting in distant precipitation. For that reason, we refer to this as a *satellite* interaction.

4. Climatological statistics of WD–TD interactions

There are enough cases in this study for us to generate provisional climatological statistics and to compare and contrast the differing interaction types. We start with analysis of the system location and timing before looking at precipitation.

a. Timing and location

First, it would be useful to know whether there are significant differences in the locations and intensities of contributing systems as a function of interaction type. To do this, we classify interactions frame-by-frame (i.e., all points on all lines inside the red box on Fig. 1, then compute the mean statistics for contributing TDs and WDs. Mean locations with interquartile ranges and mean intensities are shown in Fig. 12. Here, we consider only the main types of interaction, omitting those with a small sample size or which are more accurately described as contributing factors (e.g., secondary system, onset vortices) rather than distinct interaction types.

As vortex mergers (light blue) require the two interacting systems to be close, it is unsurprising that this is the interaction type with the smallest mean distance between WD and TD. We also see that the TD location has higher variance compared to those of other interaction types, presumably in part due to those types (cf. TD-to-WD moisture exchange, jet-streak excitation) requiring a more precise interaction angle.

The relative positioning of systems in jet-streak excitation cases (dark blue) is quite similar to those of vortex mergers, though the interaction axis is much more zonal. These cases also have the highest average TD intensity, likely following from the direct intensification of the TD by the ascending air associated with the jet-streak entrance. In general, TDs that undergo dynamically coupled interactions are on average significantly stronger than those that undergo moisture exchange interactions.

TD-to-WD moisture exchange interactions (yellow; orange for bifurcation) allow the systems to be more distant from each other and typically have comparatively stronger WDs, and as we have already seen, weaker TDs. This is particularly evident for WDs present in TD-to-WD moisture exchange bifurcation interactions, which are on average about 25% stronger than those involved in other interaction types (among the 59 case studies). This is evidence in support of our hypothesis in section 3b(1)(i) that bifurcation cases are caused by circulation associated with strong WDs advecting moisture away from weak TDs.

The mean separation and intensity of systems contributing to WD-to-TD moisture exchange interactions (green) differs little from those in TD-to-WD moisture exchange cases, except for a much weaker WD, on average the weakest of any

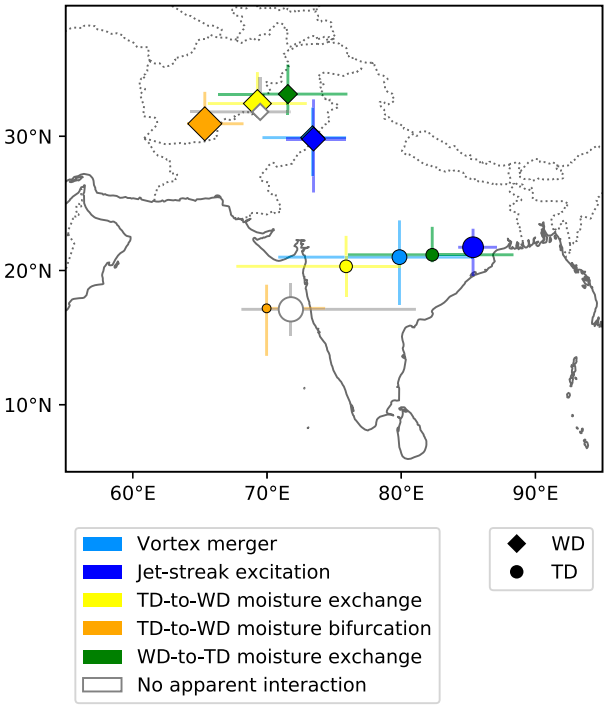

FIG. 12. Mean location of TD (circles) and WD (diamonds) during each of the main interaction categories. Error bars indicate the interquartile ranges of longitude and latitude. Marker size is proportional to the mean intensity of the system in question, calculated using 850-hPa relative vorticity for TDs and 350-hPa relative vorticity for WDs.

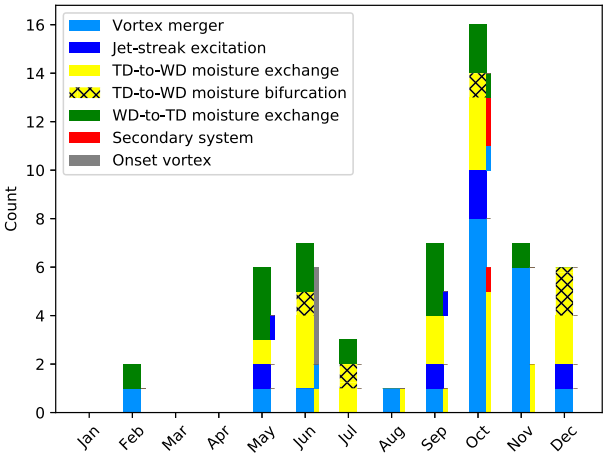

FIG. 13. Bar chart showing the seasonality of interaction types. Where a second type (or notable context) is also associated with an event, these are shown to the right of their primary type by a thinner bar.

interacting types, and a more eastward-located TD. These differences are slight, however, and it remains unclear what causes a TD-to-WD moisture exchange interaction to happen preferentially over a WD-to-TD one, or vice versa. For the cases in which no interaction is observed (white), the associated WD is typically very weak and positioned almost due north of the TD, which in contrast, is strong.

Next, we turn our attention to the seasonality of different interactions, which can shed light on the role of the large-scale environment and provide additional information for forecasters. Before we discuss this in detail, it is worth noting the seasonal cycle of contributing systems for this region. WDs can occur at any time of year, but are both stronger and more frequent during winter December–April (Hunt et al. 2018a) and weaker and less frequent during the monsoon. Data from the India Meteorological Department (IMD) Cyclone eAtlas[1] show that TDs are prevalent for much of the year, particularly from April–December. They peak in August at the height of the monsoon, but tropical cyclones peak either side of the monsoon, in May and November.

These combine to make interactions between WDs and TDs most common between May and December (Fig. 13) with a downturn during the monsoon season, when WDs are typically rare and too far north, and a large peak in October, when both types of system are relatively common. No type appears to deviate much from the mean seasonality, though it is notable that the largest contributor to the October peak is from vortex mergers, with other types being more symmetrically distributed either side of the monsoon. The disproportionately high frequency of vortex mergers in October and November comes about as the southward movement of the subtropical jet following the monsoon withdrawal brings WDs across the subcontinent; at the same time, the postmonsoon Bay of Bengal is still rich for tropical cyclogenesis. All secondary-system events happen in October, and by definition, all onset vortex events happen in June, where they dominate the population of that month. Only 2 of the 59 cases occur from January to April.

b. *Precipitation*

We have already seen that WD–TD interactions are anecdotally responsible for heavy precipitation, flooding, and loss of life, but we have not yet compared precipitation between interaction types. Figure 14 shows the mean precipitation over the 59 cases considered here, stratified by interaction type. It also shows the mean precipitation for the same domain for all WDs, all TDs, and all potential interactions (i.e., anything on the heatmap in Fig. 1, not just events in the red box). There are two caveats, which we will address in due course: first, by construction, our cases have either a strong WD or TD or both, so comparison with the full climatology of either is not strictly fair; second, as we have seen, the seasonality does not vary much by interaction type, but it is markedly different from those of WDs and TDs, respectively. Despite this, there are a number of useful inferences we can make from Fig. 14.

The heaviest precipitation by far is associated with jet-streak excitation events, and it is concentrated in the region where TDs are located during the interaction (Fig. 12), further supporting the hypothesized mechanism for this interaction. Given that a vortex merger also intensifies the TD, we might have expected similarly high precipitation values in the top-left

[1] http://www.rmcchennaieatlas.tn.nic.in/

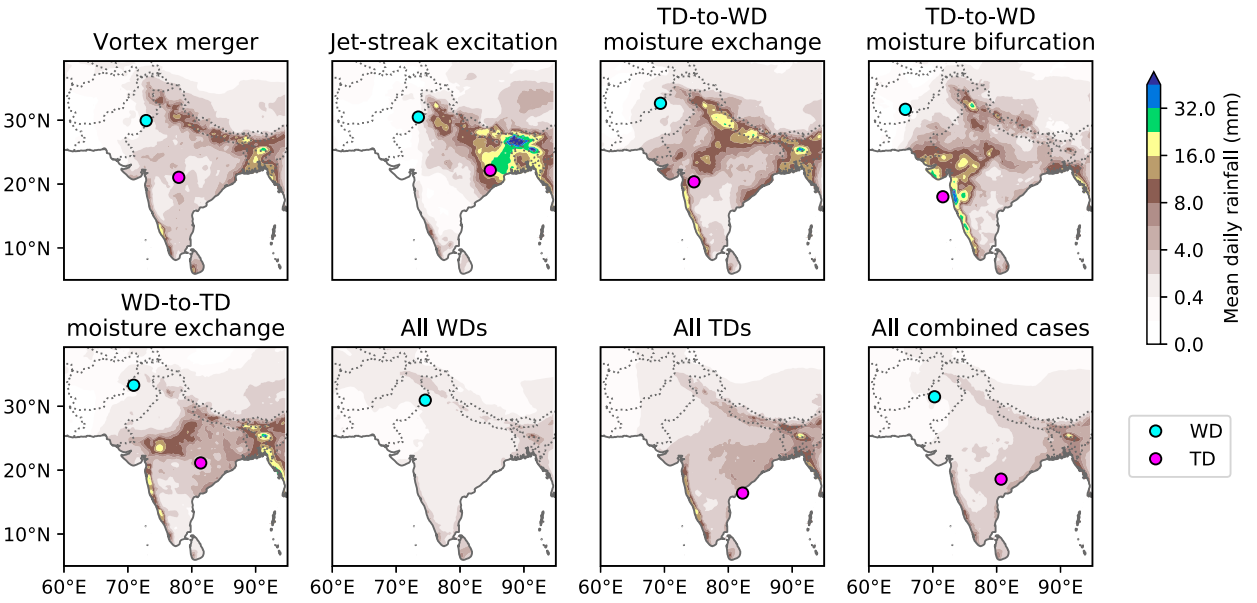

FIG. 14. Mean precipitation (from APHRODITE) over land (mm day^{-1}) for each of the major interaction types (over the 59 events) discussed in this study. For comparison, mean precipitation is also shown for all WDs, all TDs, and all days where both are simultaneously present in the domain (see Fig. 1 for reference). The mean location of WDs and TDs for each set are given by cyan and magenta markers, respectively.

panel of Fig. 14. There are several possible reasons that we do not observe that: first, the greatly increased spatial variance of TDs when compared with jet-streak excitation cases; second, a considerable number of mergers happen over or near the Himalayan foothills when the TD is already close to the end of its life, giving it less chance to deepen to the same extent.

Precipitation in TD-to-WD moisture exchange cases is consistent with the mechanism outlined in section 1, falling most heavily in and around the orography to the north where WDs usually precipitate (cf. the panel showing all WDs). Almost all of the precipitation happens in this region during pure TD-to-WD moisture exchange interactions, supporting the notion that TDs push moisture flux toward the WDs, which then cause the precipitation. In bifurcating cases, there is also significant precipitation associated with the TD, in agreement with what we found in section 3b(1), that a WD takes only a fraction of the TD moisture flux, so the latter is still associated with significant precipitation. The mean precipitation for WD-to-TD moisture exchange interactions is focused over central and western India (with the additional orographic band over the northeast, common to all interactions), clearly linked with the TD and located to the northwest of its mean location (Fig. 12), consistent with the single case discussed in section 2 and supporting the hypothesis raised there that this kind of interaction causes rainfall to occur preferentially to the northwest of the TD. These results are confirmed using precipitation data from the IMDAA reanalysis (Fig. S9).

These footprints provide some useful evidence to support our earlier hypotheses in section 3—that rainfall is amplified by a dynamical coupling interaction but relocated by a moisture exchange interaction—but they do not permit a fair comparison to judge differences in magnitude between interaction types. To do this, we construct probability density functions (Fig. 15) of all daily rainfall amounts at each pixel (0.25° × 0.25°; APHRODITE). These are then separated into interaction types as well as climatologies of selected WD and TD intensity thresholds, computed using 350- and 850-hPa relative vorticity, respectively.

The precipitation distributions for each interaction type follow the all-TD climatology quite closely, with the clear exception of jet-streak excitation cases, which provide significantly heavier rainfall than even the top decile of TDs. Precipitation rates of 100–150 mm day^{-1} in vortex merger events are also significantly more common than the all-TD climatology, but there are insufficient data to extrapolate this to the highest rates. WD-to-TD moisture exchange interactions also show an increase in frequency of rates exceeding 250 mm day^{-1}, but these are too scarce in our dataset to make any meaningful generalizations. In short, we see that precipitation in dynamically coupled cases (jet-streak excitations, and to a lesser extent vortex mergers) is amplified, but precipitation in moisture exchange interactions (both WD-to-TD and TD-to-WD) is relocated.

5. Toward an automated framework

Thus far, our classification for each case has been determined manually. Here, we explore how our results might inform the development of an automatic classification and compositing framework and outline the problems and advantages of different methods. Such a framework is important for forecasters who would need to assess whether a particular

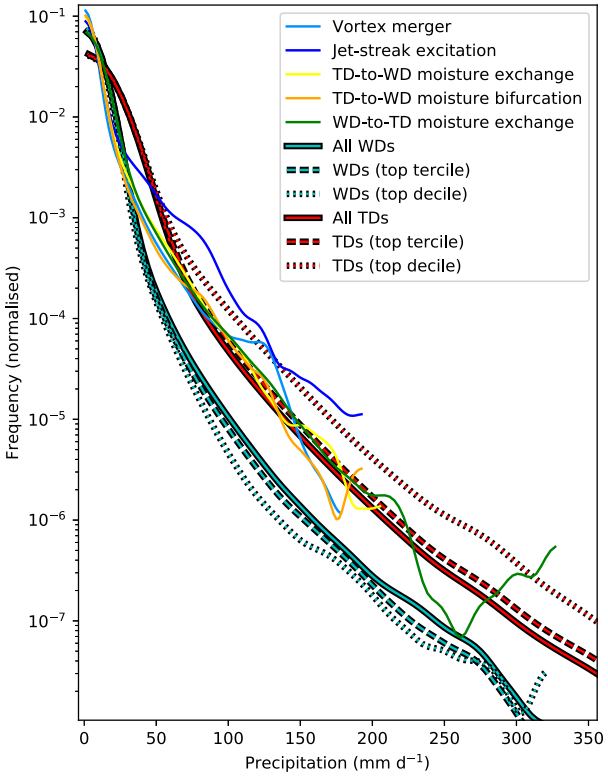

FIG. 15. Probability density functions of daily precipitation amounts over South Asia (5°–40°N, 60°–95°E; land only) by interaction type. For comparison, the distributions for all WDs and all TDs are also shown, along with respective stratification by intensity into their top tercile and top decile.

interaction is likely to occur, and whether or not there will be intense precipitation as a result. The first step to achieving this is to choose and implement an algorithm that can automatically classify different interaction types. We initially attempted to do this using a k-means clustering method. We extracted and normalized variables that were shown to be important indicators of interaction type earlier in this paper: rainfall, vertically integrated moisture flux, vertical velocity, vorticity, and upper-level winds. We concatenated these and performed dimensionality reduction. Resulting clusters exposed only differences in WD and TD locations and were not sensitive to the selection of input variables or method of dimensionality reduction. To overcome this, we rotated, rescaled, and for vector data, reorientated the input variables, so that each sample was projected onto a common grid with the TD center located at [0, 0] and the WD center located at [0, 1]. Clustering was reattempted, but remained insensitive to input parameters, instead separating clusters according to WD–TD distance. This is because the projected dynamical fields are sensitive to this value: being stretched or squashed as the projection requires.

Even had this been successful, it may not have been representative: most common clustering techniques do not permit a point to be assigned to more than one cluster, yet, as we have shown in this paper, the interaction types we have presented are not all mutually exclusive. Therefore, we decided to manually derive automatic selection methods based on our selection of case studies, which we outline below.

a. *Vortex merger*

The method for vortex mergers is based on the identification procedure used in Fig. 2b, finding cases where vorticity contours at consecutive pressure levels overlap:

1) Extract the relative vorticity ζ_k at every pressure level k from 850 to 200 hPa in intervals of 50 hPa.
2) Find contour polygons C_k^i for the $2 \times 10^{-5}\,\mathrm{s}^{-1}$ isolines at each level.
3) Identify the polygon from the set C_{850}^i that contains the center of the TD. Label this polygon C_{850}^*.
4) Identify the polygon from the set C_{800}^i that contains the largest amount of area that is also contained in C_{850}^*. Label this polygon C_{800}^*, and fraction of area of C_{850}^* that is in C_{800}^*, r_{850}.
5) Propagate through all levels, finding the polygon in the set C_k^i that contains the largest fraction of C_{k-1}^*. Retain all r_k.
6) If C_{350}^* does not contain the center of the WD, the score for this metric is 0. If it does, the score is the mean of the lowest three values in r_k.
7) A merger is determined to be occurring if the score exceeds 0.1.

b. *Jet-streak excitation*

Efforts to derive a metric based on characteristics of the Q-vector field were not fruitful. Instead, the method for jet-streak excitation interactions is based on Figs. 6 and 7, using the importance of the relative location of the TD to the jet, and the midlevel deepening of the TD:

1) Compute the T63-truncated vertical velocity ω and the normal component of the wind u_n over a vertical cross-section plane containing the centers of both the WD and the TD.
2) Locate the most negative value of 500-hPa ω coincident with the plane within 250 km of the TD center. Call this quantity ω^*.
3) Locate the largest value of 250-hPa u_n between the TD and WD centers, i.e., the center of the jet (should it exist there). Call this quantity u_n^*.
4) Project the locations of ω^* and u_n^* to the surface and calculate the length of the geodesic separating them, δ.
5) The score for this metric is then calculated as $-100[\omega^*(u_n^* - 20)]/\delta$, assuming all quantities are in SI units. If the score for the vortex merger metric above is nonzero, then the score for this metric is set to 0.
6) A jet-streak excitation is determined to be occurring if the score exceeds $0.2\,\mathrm{Pa\,s}^{-2}$.

c. *Moisture exchange interactions*

This method is based on the moisture flux analysis associated with Fig. 8. Here we use the common projection outlined above, whereby all fields are rescaled and rotated such that the TD center is located at [0, 0] and the WD center is located

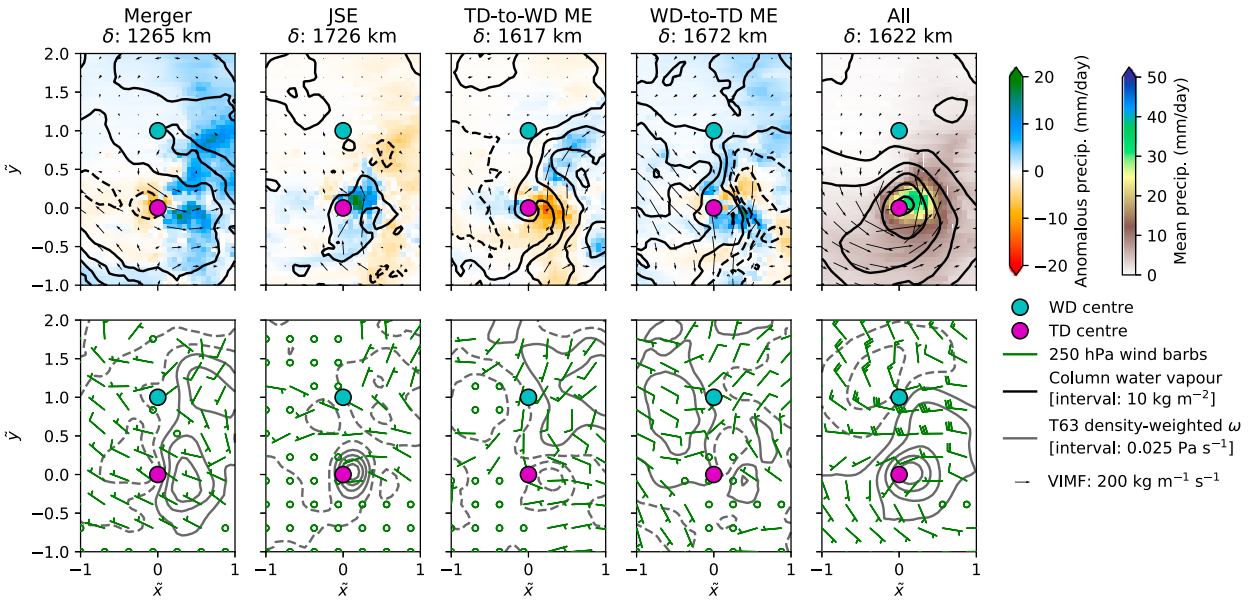

FIG. 16. Standardized composites for automatically identified interaction types. For each time step included in each composite, data are rotated and rescaled such that the TD center is located at [0, 0] and the WD center is located at [0, 1]. (right) The mean values for all interactions (i.e., across all 59 cases in this paper), and each interaction type is then presented as an anomaly to this mean. Magnitudes quoted in the legend for ω and vertically integrated moisture flux are used in the mean composite, whereas the anomaly panels use half this value. (top) Rainfall (using IMDAA reanalysis), vertically integrated moisture flux, and column water vapor (solid lines indicating a positive anomaly; dashed lines indicating a negative anomaly). (bottom) The 250-hPa winds and T63-filtered density-weighted vertical velocity averaged over the atmospheric column (solid lines showing ascent or anomalous ascent; dashed lines showing descent or anomalous descent). The δ value indicates the mean separation of system centers for each interaction type.

at [0, 1]. Let us call the axes of this common coordinate system $\tilde{x}$ and $\tilde{y}$.

1) Project vertically integrated moisture flux and daily precipitation (in this case, we use reanalyzed precipitation data from IMDAA) onto the common grid. Call these quantities $\tilde{f}$ and $\tilde{p}$, respectively.
2) Compute the mean of the $\tilde{y}$ component of $\tilde{f}$ over all grid points where that component is positive (i.e., the mean magnitude of southerly flux), bounded by $-1 \le \tilde{x} \le 1$ and $0 \le \tilde{y} \le 1$. Call this quantity $\tilde{f}_y^+$; it approximates the moisture flux passing from the TD to the WD. Do the same for grid points where the $\tilde{y}$ component is negative to compute $\tilde{f}_y^-$; this approximates the moisture flux passing from the WD to the TD.
3) Compute the mean of $\tilde{p}$ in the region bounded by $-1 \le \tilde{x} \le 1$ and $-0.5 \le \tilde{y} \le 0.5$. Call this quantity $\tilde{p}_t$; it represents precipitation associated with the TD.
4) Compute the mean of $\tilde{p}$ in the region bounded by $-1 \le \tilde{x} \le 1$ and $0.5 \le \tilde{y} \le 1.5$. Call this quantity $\tilde{p}_w$; it represents precipitation associated with the WD.
5) The score for the TD-to-WD moisture exchange metric is then given by $\tilde{f}_y^+ \tilde{p}_w$, and for the WD-to-TD moisture exchange metric by $\tilde{f}_y^- \tilde{p}_t$. Where the TD-to-WD moisture exchange score exceeds $0.25\,\mathrm{mm\,day^{-1}\,kg\,m^{-1}\,s^{-1}}$ ($2.9 \times 10^{-9}\,\mathrm{kg\,s^{-2}}$), we determine a TD-to-WD moisture exchange interaction to be occurring. Where the WD-to-TD moisture exchange score exceeds $1\,\mathrm{mm\,day^{-1}\,kg\,m^{-1}\,s^{-1}}$ ($1.2 \times 10^{-8}\,\mathrm{kg\,s^{-2}}$), we determine a WD-to-TD moisture exchange interaction to be occurring. The asymmetry in these thresholds derives from TDs typically being associated with much greater precipitation than WDs.

When compared against the manual classifications given in Table S1, these metrics perform relatively well, matching about 70% of moisture exchange and vortex merger cases, and about 50% of jet-streak excitation cases. In particular, we find that the automatic method identifies about twice as many jet-streak excitation cases as did our manual method because it captured configurations that we did not recognize during the manual process.

Using the automatic results, we use the common projection to composite selected variables in Fig. 16. Many of the features discussed in the previous sections are present. For vortex mergers there is enhanced cyclonic circulation around both systems as a whole, with associated enhanced ascent. The strong jet separating the WD and TD is clearly visible in the jet-streak excitation composite, along with the strongest ascent and precipitation of any of the interaction types. The TD-to-WD moisture exchange composite shows anomalous moisture flux passing from the TD to the WD, over a region of anomalous ascent, resulting in an increase in anomalous column water vapor and precipitation near the WD. Interestingly, 39% of jet-streak excitation interactions were also classified as TD-to-WD moisture exchanges, and 37% of TD-to-WD moisture exchange cases were also classified as having a jet-streak excitation. These values were 6% and 8%, respectively, for the overlap between jet-streak excitations and WD-to-TD

moisture exchange interactions. The WD-to-TD moisture exchange composite shows anomalous moisture flux entering the TD, with a significant proportion coming from the WD. This results in regions of anomalous positive precipitation near the TD.

We reiterate that these automatic metrics are only presented as guidelines, and further work is needed to check whether they are robust. For example, the moisture exchange metrics may be unreliable over larger interaction distances, where mean flux would be a less useful indicator of whether moisture is being advected from one system to another. Likewise, we must note that despite being an acceptable compromise, the common projection method suffers from the smearing out of geographically fixed features such as orographic rainfall.

6. Discussion

The most significant shortcoming of this study is that classifications were made manually, largely by inspection of synoptic charts and vorticity and moisture budgets. While we have defined criteria that can be used for automatic classification, future studies that seek to expand or improve our climatology should focus on the further development of automated classification techniques. Since this is a classification problem, it could be addressed using machine learning techniques. Algorithm-based identification is a potentially complex problem for moisture exchange interactions that may require intelligent use of moisture trajectory analyses.

As we discussed in the Introduction, several early observational studies noted how passing WDs could intensify an immature TD in the Bay of Bengal; however, the intensity criterion in our case study selection method essentially omits such interactions from our analysis. These would presumably be more prevalent in an extended climatology, either appearing as vortex mergers or an as-yet-unnamed dynamically coupled interaction. Similarly, we subjectively dismissed several cases as not involving a detectable interaction. This does not necessarily mean that they do not interact, and more work will be needed to detect and determine these potential pathways.

We also dismissed any cases of TDs spawning directly from strong WDs, arguing that this does not constitute an interaction between a tropical and extratropical system. The TD tracking algorithm does not make this distinction, so these events—five in all satisfying our remaining criteria—were removed. Several studies have highlighted the importance of these WD-born TDs (Pisharoty and Desai 1956; Chakravarti 1968; Loe et al. 2005), but to what extent they are genuinely ''tropical'' remains an open question.

Previous work on the interactions between TCs and UTTs found that for certain TC–UTT orientations and UTT characteristics, the resulting wind shear was detrimental to TC growth and the interaction therefore weakened, rather than intensified, the TC (DeMaria et al. 1993; Molinari et al. 1998). We assumed that this would not be a factor in WD–TD interactions because strong vertical wind shear is thought to be either beneficial for or otherwise not significantly detrimental to TD growth (Rao et al. 2004; Ditchek et al. 2016). This assumption was supported by the fact that in none of the 59 cases explored here did the TD appear to weaken during interaction with a WD. Nevertheless, vertical wind shear could play an important role in the magnitude of TD intensification and should be a subject of future study.

Aside from those listed above, there are a number of important avenues for potential future work, many of which would be greatly assisted by the development of an extended climatology of events. For example, why do some TD–WD pairs not interact, despite being sufficiently strong and proximal? What is the role of TD-added moisture in increasing the instability around a WD during TD-to-WD moisture exchange interactions, and what role do fronts and baroclinic zones actually play in such cases? How important is orography in interactions that increase WD precipitation?

7. Conclusions

While tropical depressions (TDs) largely occur during summer months and extratropical western disturbances (WDs) largely occur during winter, both can cause heavy precipitation outside these periods, and can even coincide—most notoriously during the north India floods of 2013.

In this study, existing databases of WD tracks and TD tracks were used to identify instances of WD–TD interactions. The interactions were filtered using proximity and intensity criteria, leaving 59 case studies (Table S1) to be examined in detail, with selected examples being given for each of the four interaction types identified in this paper.

The 59 cases could be broadly separated into two main families: dynamical coupling and moisture exchange. These are more usefully subdivided into four distinct subtypes that are not necessarily mutually exclusive. Schematics of each type are given in Fig. 17, which we describe below:

a. Vortex merger

These interactions occur when the TD and WD vortices physically merge into a single vortex, usually as a result of the TD moving northward into the ascent region found to the east of the WD center. This results in upward vertical advection of vorticity, strengthening the WD directly and the TD through stretching. These are dynamically coupled interactions and typically occur (though not always) around the Himalayan foothills. Merger interactions are an analog to the ''favorable superposition'' interactions of Hanley et al. (2001) and the cutoff cluster of Fischer et al. (2019).

b. Jet-streak excitation

These interactions occur when a WD disrupts the subtropical jet enough to form a jet streak downstream. Entrances to these jet streaks induce a region of broad, strong ascent to their right (i.e., south or southeast in the Northern Hemisphere). TDs entering this region quickly and dramatically intensify in response to the additional ageostrophic forcing. These are also dynamically coupled, and result in the highest rainfall rates of any interaction type. Jet-streak excitation interactions are an analog to the ''favorable distant interactions'' of

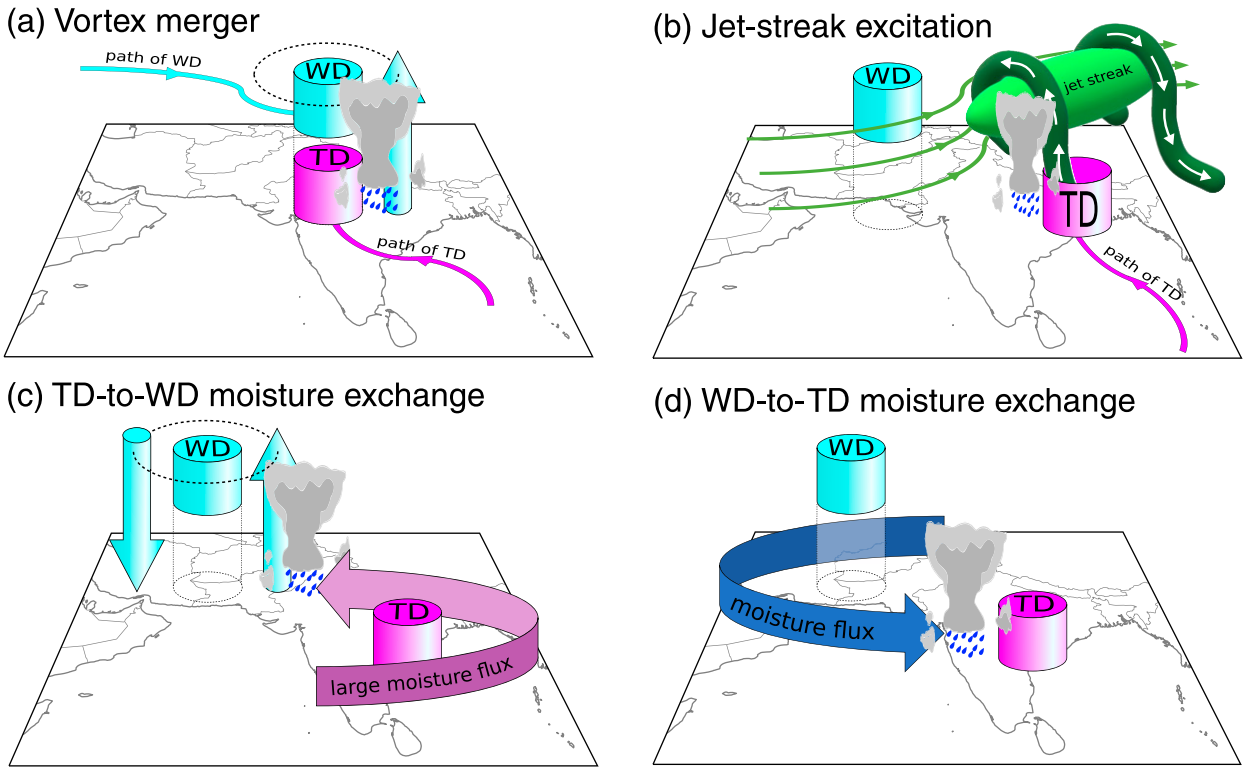

FIG. 17. Schematics for each of the major interaction types identified in this paper.

Hanley et al. (2001) and the northwest UTT cluster of Fischer et al. (2019).

c. TD-to-WD moisture exchange

These interactions are the first and most common of the three types in the moisture exchange family. When situated at the correct relative angle, TDs can propel southerly/southwesterly moisture flux toward a WD where it is precipitated either in the area of ascent associated with WDs (to their east), or over the orography. TD-to-WD moisture exchange interactions can result in very high precipitation rates over north India and Pakistan, the 2013 Uttarakhand floods being the most significant among them. This type of moisture exchange is dynamically similar to the predecessor rainfall events identified in Galarneau et al. (2010). Even if the WD and TD are not correctly orientated, a sufficiently strong WD is able to draw moisture away from the TD (''bifurcating'' its moisture flux). As a result of this split, the TD is still associated with some heavy rainfall, and precipitation near the WD is slightly reduced when compared to a standard TD-to-WD moisture exchange interaction.

d. WD-to-TD moisture exchange

These work in the opposite manner to TD-to-WD moisture exchange: WDs provide or direct northerly/northwesterly moisture flux to the TD. Around 10%–20% of the total moisture consumed by the TD originates from the WD, in contrast to TD-to-WD moisture exchange interactions where nearly all of the moisture flux consumed by the WD is provided by the TD. There is some evidence of an increase in high rainfall rates when compared to noninteracting TDs, which typically occur over central or east India.

Six of the 59 cases appeared not to contain an interaction between the TD and WD. None of the 59 cases contained an ''unfavorable'' interaction. In Fischer et al. (2019), unfavorable interactions depended on the upper-tropospheric trough imparting large wind shear over the tropical cyclone. While that situation is possible in WD–TD configurations over South Asia, vertical wind shear is not detrimental to the growth of TDs as it is in TCs.

The monthly frequency of interactions was found to be bimodal with peaks either side of the monsoon in June and October, the latter being by far the most populous month. Vortex mergers are disproportionately common in October, but the other interaction types did not appear to feature pronounced seasonality. Monsoon onset vortices were a very important contributor to interactions in June, and the several cases of two systems interacting almost simultaneously with a third were confined to October.

Automatic criteria to identify each type of interaction were proposed. For vortex mergers, this depended on overlapping regions of high vorticity at each pressure level. For jet-streak excitations, the criterion was derived from the strength of the jet, midlevel ascent, and the relative positioning of the WD and jet. For both types of moisture exchange interactions, the criteria were based on vertically integrated moisture flux

projected onto the vector connecting the system centers. These metrics performed well when compared with the manually identified classifications, although the automatic method identified considerably more jet-streak excitations.

A common composite projection was proposed as a consistent framework to compare different interaction types, regardless of the absolute and relative positions of the contributing TD and WD. Combining this with the automatic criteria, an automatic climatology was presented, in which the key results from the manual climatology were ratified.

Acknowledgments. This work and its contributions (KMRH, AGT, RKHS) were conducted through the Weather and Climate Science for Service Partnership (WCSSP) India, a collaborative initiative between the Met Office, supported by the U.K. Government's Newton Fund, and the Indian Ministry of Earth Sciences (MoES). KMRH wishes to thank Thorwald Stein at the University of Reading and Andrew Ross at the University of Leeds for their constructive comments on this research. AGT acknowledges the INCOMPASS project funded by the Natural Environment Research Council (Grant NE/P003117/1). KMRH also wishes to thank Chief Editor David Schultz and three anonymous reviewers for the considerable time they spent in offering suggestions to improve the clarity and direction of this manuscript.

Data availability statement. ERA-Interim reanalysis data used in this study are publicly available at https://www.ecmwf.int/en/forecasts/datasets/reanalysis-datasets/era-interim. APHRODITE-2 gauge rainfall data are publicly available at http://aphrodite.st.hirosaki-u.ac.jp/download/. IMDAA reanalysis data are publicly available at https://rds.ncmrwf.gov.in/. The database of WD tracks is publicly available at http://dx.doi.org/10.5285/233cf64c54e946e0bb691a07970ec245. The database of TD tracks used in this study is publicly available at http://gws-access.jasmin.ac.uk/public/incompass/kieran/track_data/lps-tracks_v1_1979-2014.csv.

REFERENCES

Adames, Á. F., 2021: Interactions between water vapor, potential vorticity, and vertical wind shear in quasi-geostrophic motions: Implications for rotational tropical motion systems. *J. Atmos. Sci.*, **78**, 903–923, https://doi.org/10.1175/JAS-D-20-0205.1.

——, and Y. Ming, 2018: Moisture and moist static energy budgets of South Asian monsoon low pressure systems in GFDL AM4. 0. *J. Atmos. Sci.*, **75**, 2107–2123, https://doi.org/10.1175/JAS-D-17-0309.1.

Akilan, A., S. Balaji, K. K. A. Azeez, and M. Satyanarayanan, 2017: Source and causes of 2015 great pluvial flood of Chennai, Tamil Nadu, and its surroundings. *J. Geol. Soc. India*, **90**, 602–608, https://doi.org/10.1007/s12594-017-0758-9.

Ali, A., and J. U. Chowdhury, 1997: Tropical cyclone risk assessment with special reference to Bangladesh. *Mausam*, **48**, 305–322.

Arulalan, T., K. AchutaRao, K. M. R. Hunt, A. G. Turner, A. K. Mitra, and A. Sarkar, 2020: Prediction of western disturbances tracks using NEPS. NCMRWF, 3 pp., https://www.ncmrwf.gov.in/event/emmda/Abstracts/TArulalan_Abstract_EMMDA.pdf.

Ashrit, R., and Coauthors, 2020: IMDAA regional reanalysis: Performance evaluation during Indian summer monsoon season. *J. Geophys. Res. Atmos.*, **125**, e2019JD030973, https://doi.org/10.1029/2019JD030973.

Baisya, H., S. Pattnaik, and P. V. Rajesh, 2017: Land surface-precipitation feedback analysis for a landfalling monsoon depression in the Indian region. *J. Adv. Model. Earth Syst.*, **9**, 712–726, https://doi.org/10.1002/2016MS000829.

Boos, W. R., J. V. Hurley, and V. S. Murthy, 2015: Adiabatic westward drift of Indian monsoon depressions. *Quart. J. Roy. Meteor. Soc.*, **141**, 1035–1048, https://doi.org/10.1002/qj.2454.

Bosart, L. F., W. E. Bracken, J. Molinari, C. S. Velden, and P. G. Black, 2000: Environmental influences on the rapid intensification of Hurricane Opal (1995) over the Gulf of Mexico. *Mon. Wea. Rev.*, **128**, 322–352, https://doi.org/10.1175/1520-0493(2000)128<0322:EIOTRI>2.0.CO;2.

Bracken, W. E., and L. F. Bosart, 2000: The role of synoptic-scale flow during tropical cyclogenesis over the North Atlantic Ocean. *Mon. Wea. Rev.*, **128**, 353–376, https://doi.org/10.1175/1520-0493(2000)128<0353:TROSSF>2.0.CO;2.

Cannon, F., L. M. V. Carvalho, C. Jones, and J. Norris, 2016: Winter westerly disturbance dynamics and precipitation in the western Himalaya and Karakoram: A wave-tracking approach. *Theor. Appl. Climatol.*, **125**, 27–44, https://doi.org/10.1007/s00704-015-1489-8.

Chakravarti, A. K., 1968: Summer rainfall India: A review of monsoonal and extramonsoonal aspects—II. *Atmosphere*, **6**, 87–114, https://doi.org/10.1080/00046973.1968.9676553.

Chen, T.-C., J.-H. Yoon, and S.-Y. Wang, 2005: Westward propagation of the Indian monsoon depression. *Tellus*, **57A**, 758–769, https://doi.org/10.1111/j.1600-0870.2005.00140.x.

Chevuturi, A., and A. P. Dimri, 2016: Investigation of Uttarakhand (India) disaster-2013 using weather research and forecasting model. *Nat. Hazards*, **82**, 1703–1726, https://doi.org/10.1007/s11069-016-2264-6.

Clark, S. K., Y. Ming, and Á. F. Adames, 2020: Monsoon low pressure system–like variability in an idealized moist model. *J. Climate*, **33**, 2051–2074, https://doi.org/10.1175/JCLI-D-19-0289.1.

Dee, D. P., and Coauthors, 2011: The ERA-Interim reanalysis: Configuration and performance of the data assimilation system. *Quart. J. Roy. Meteor. Soc.*, **137**, 553–597, https://doi.org/10.1002/qj.828.

DeMaria, M., 1996: The effect of vertical shear on tropical cyclone intensity change. *J. Atmos. Sci.*, **53**, 2076–2088, https://doi.org/10.1175/1520-0469(1996)053<2076:TEOVSO>2.0.CO;2.

——, J. Kaplan, and J.-J. Baik, 1993: Upper-level eddy angular momentum fluxes and tropical cyclone intensity change. *J. Atmos. Sci.*, **50**, 1133–1147, https://doi.org/10.1175/1520-0469(1993)050<1133:ULEAMF>2.0.CO;2.

Diaz, M., and W. R. Boos, 2019: Monsoon depression amplification by moist barotropic instability in a vertically sheared environment. *Quart. J. Roy. Meteor. Soc.*, **145**, 2666–2684, https://doi.org/10.1002/qj.3585.

——, and ——, 2021: Evolution of idealized vortices in monsoon-like shears: Application to monsoon depressions. *J. Atmos. Sci.*, **78**, 1207–1225, https://doi.org/10.1175/JAS-D-20-0286.1.

Dimri, A. P., and A. Chevuturi, 2014: Model sensitivity analysis study for western disturbances over the Himalayas. *Meteor. Atmos. Phys.*, **123**, 155–180, https://doi.org/10.1007/s00703-013-0302-4.

——, and ——, 2016: Western disturbances—Structure. *Western Disturbances—An Indian Meteorological Perspective*, Springer, 1–26.

Ditchek, S. D., W. R. Boos, S. J. Camargo, and M. K. Tippett, 2016: A genesis index for monsoon disturbances. *J. Climate*, **29**, 5189–5203, https://doi.org/10.1175/JCLI-D-15-0704.1.

Dong, W.-H., Y. Ming, and V. Ramaswamy, 2020: Projected changes in South Asian monsoon low pressure systems. *J. Climate*, **33**, 7275–7287, https://doi.org/10.1175/JCLI-D-20-0168.1.

Dutta, D., A. Routray, D. P. Kumar, J. P. George, and V. Singh, 2019: Simulation of a heavy rainfall event during southwest monsoon using high-resolution NCUM-modeling system: A case study. *Meteor. Atmos. Phys.*, **131**, 1035–1054, https://doi.org/10.1007/s00703-018-0619-0.

EM-DAT, 2020: The emergency events database. Université catholique de Louvain (UCL), D. Guha Sapir, Brussels, Belgium, accessed 3 March 2020, www.emdat.be.

Emanuel, K. A., 1986: An air–sea interaction theory for tropical cyclones. Part I: Steady-state maintenance. *J. Atmos. Sci.*, **43**, 585–605, https://doi.org/10.1175/1520-0469(1986)043<0585:AASITF>2.0.CO;2.

——, C. DesAutels, C. Holloway, and R. Korty, 2004: Environmental control of tropical cyclone intensity. *J. Atmos. Sci.*, **61**, 843–858, https://doi.org/10.1175/1520-0469(2004)061<0843:ECOTCI>2.0.CO;2.

Fischer, M. S., B. H. Tang, and K. L. Corbosiero, 2017: Assessing the influence of upper-tropospheric troughs on tropical cyclone intensification rates after genesis. *Mon. Wea. Rev.*, **145**, 1295–1313, https://doi.org/10.1175/MWR-D-16-0275.1.

——, ——, and ——, 2019: A climatological analysis of tropical cyclone rapid intensification in environments of upper-tropospheric troughs. *Mon. Wea. Rev.*, **147**, 3693–3719, https://doi.org/10.1175/MWR-D-19-0013.1.

Fujiwhara, S., 1921: The natural tendency towards symmetry of motion and its application as a principle in meteorology. *Quart. J. Roy. Meteor. Soc.*, **47**, 287–292, https://doi.org/10.1002/qj.49704720010.

Galarneau, T. J., Jr., L. F. Bosart, and R. S. Schumacher, 2010: Predecessor rain events ahead of tropical cyclones. *Mon. Wea. Rev.*, **138**, 3272–3297, https://doi.org/10.1175/2010MWR3243.1.

——, R. McTaggart-Cowan, L. F. Bosart, and C. A. Davis, 2015: Development of North Atlantic tropical disturbances near upper-level potential vorticity streamers. *J. Atmos. Sci.*, **72**, 572–597, https://doi.org/10.1175/JAS-D-14-0106.1.

George, C. J., and R. K. Datta, 1965: A synoptic study of monsoon depression in the month of September 1963. *Indian J. Meteor. Geophys.*, **16**, 213–220.

Godbole, R. V., 1977: The composite structure of the monsoon depression. *Tellus*, **29**, 25–40, https://doi.org/10.1111/j.2153-3490.1977.tb00706.x.

Gray, W. M., 1985: Tropical cyclone global climatology. Tech. Rep. 1, WMO, 19 pp.

Hanley, D., J. Molinari, and D. Keyser, 2001: A composite study of the interactions between tropical cyclones and upper-tropospheric troughs. *Mon. Wea. Rev.*, **129**, 2570–2584, https://doi.org/10.1175/1520-0493(2001)129<2570:ACSOTI>2.0.CO;2.

Haynes, P. H., and M. E. McIntyre, 1987: On the evolution of vorticity and potential vorticity in the presence of diabatic heating and frictional or other forces. *J. Atmos. Sci.*, **44**, 828–841, https://doi.org/10.1175/1520-0469(1987)044<0828:OTEOVA>2.0.CO;2.

Houze, R. A., L. A. McMurdie, K. L. Rasmussen, A. Kumar, and M. M. Chaplin, 2017: Multiscale aspects of the storm producing the June 2013 flooding in Uttarakhand, India. *Mon. Wea. Rev.*, **145**, 4447–4466, https://doi.org/10.1175/MWR-D-17-0004.1.

Hunt, K. M. R., and J. K. Fletcher, 2019: The relationship between Indian monsoon rainfall and low-pressure systems. *Climate Dyn.*, **53**, 1859–1871, https://doi.org/10.1007/s00382-019-04744-x.

——, and A. Menon, 2019: The 2018 Kerala floods: A climate change perspective. *Climate Dyn.*, **54**, 2433–2446, https://doi.org/10.1007/S00382-020-05123-7.

——, A. G. Turner, and D. E. Parker, 2016: The spatiotemporal structure of precipitation in Indian monsoon depressions. *Quart. J. Roy. Meteor. Soc.*, **142**, 3195–3210, https://doi.org/10.1002/qj.2901.

——, ——, and L. C. Shaffrey, 2018a: The evolution, seasonality, and impacts of western disturbances. *Quart. J. Roy. Meteor. Soc.*, **144**, 278–290, https://doi.org/10.1002/qj.3200.

——, ——, and ——, 2018b: Extreme daily rainfall in Pakistan and north India: Scale-interactions, mechanisms, and precursors. *Mon. Wea. Rev.*, **146**, 1005–1022, https://doi.org/10.1175/MWR-D-17-0258.1.

——, ——, and ——, 2019a: BITMAP: Tracks of western disturbances transiting over Pakistan and North India in Era-Interim reanalysis data (1979-2015). Centre for Environmental Data Analysis (CEDA), accessed 3 March 2020, https://doi.org/10.5285/233CF64C54E946E0BB691A07970EC245.

——, ——, and ——, 2019b: Representation of western disturbances in CMIP5 models. *J. Climate*, **32**, 1997–2011, https://doi.org/10.1175/JCLI-D-18-0420.1.

Hurley, J. V., and W. R. Boos, 2015: A global climatology of monsoon low pressure systems. *Quart. J. Roy. Meteor. Soc.*, **141**, 1049–1064, https://doi.org/10.1002/qj.2447.

Joseph, P. V., 1978: Sub-tropical westerlies in relation to large scale failure of Indian monsoon. *Indian J. Meteor. Hydrol. Geophys.*, **29**, 412–418.

——, 1981: Ocean-atmosphere interaction on a seasonal scale over north Indian Ocean and Indian monsoon rainfall and cyclone tracks: A preliminary study. *Mausam*, **32**, 237–246.

Joseph, S., and Coauthors, 2015: North Indian heavy rainfall event during June 2013: Diagnostics and extended range prediction. *Climate Dyn.*, **44**, 2049–2065, https://doi.org/10.1007/s00382-014-2291-5.

Kalsi, S. R., 1980: On some aspects of interaction between middle latitude westerlies and monsoon circulation. *Mausam*, **31**, 305–308.

——, and R. K. Jain, 1989: On some aspects of marginal cyclones. *Mausam*, **40**, 47–50.

——, and S. R. Halder, 1992: Satellite observations of interaction between tropics and mid-latitudes. *Mausam*, **43**, 59–64.

Komaromi, W. A., and J. D. Doyle, 2018: On the dynamics of tropical cyclone and trough interactions. *J. Atmos. Sci.*, **75**, 2687–2709, https://doi.org/10.1175/JAS-D-17-0272.1.

Krishnamurti, T. N., P. Ardanuy, Y. Ramanathan, and R. Pasch, 1981: On the onset vortex of the summer monsoon. *Mon. Wea. Rev.*, **109**, 344–363, https://doi.org/10.1175/1520-0493(1981)109<0344:OTOVOT>2.0.CO;2.

Lander, M., and G. J. Holland, 1993: On the interaction of tropical-cyclone-scale vortices. I: Observations. *Quart. J. Roy. Meteor. Soc.*, **119**, 1347–1361, https://doi.org/10.1002/qj.49711951406.

Lang, T. J., and A. P. Barros, 2004: Winter storms in the central Himalayas. *J. Meteor. Soc. Japan*, **82**, 829–844, https://doi.org/10.2151/jmsj.2004.829.

Leroux, M.-D., M. Plu, and F. Roux, 2016: On the sensitivity of tropical cyclone intensification under upper-level trough forcing. *Mon. Wea. Rev.*, **144**, 1179–1202, https://doi.org/10.1175/MWR-D-15-0224.1.

Lewis, B. M., and D. P. Jorgensen, 1978: Study of the dissipation of Hurricane Gertrude (1974). *Mon. Wea. Rev.*, **106**,

1288–1306, https://doi.org/10.1175/1520-0493(1978)106<1288:SOTDOH>2.0.CO;2.

Loe, B. R., M. Ali, and D. Joardar, 2005: Synoptic systems associated with onset of southwest monsoon over Rajasthan. *Mausam*, **56**, 857.

Madhura, R. K., R. Krishnan, J. V. Revadekar, M. Mujumdar, and B. N. Goswami, 2015: Changes in western disturbances over the western Himalayas in a warming environment. *Climate Dyn.*, **44**, 1157–1168, https://doi.org/10.1007/s00382-014-2166-9.

Malurkar, S. L., 1947: Abnormally dry and wet western disturbances over North India. *Curr. Sci.*, **16**, 139–141.

Martin, G. M., and Coauthors, 2019: Forecasting the monsoon on daily to seasonal time-scales in support of a field campaign. *Quart. J. Roy. Meteor. Soc.*, **146**, 2906–2927, https://doi.org/10.1002/qj.3620.

Martin, J. E., 2006: *Mid-Latitude Atmospheric Dynamics: A First Course*. 1st ed. Wiley-Blackwell, 336 pp.

Midhuna, T. M., P. Kumar, and A. P. Dimri, 2020: A new western disturbance index for the Indian winter monsoon. *J. Earth Syst. Sci.*, **129**, 59, https://doi.org/10.1007/s12040-019-1324-1.

Mishra, A., 2015: Cloudburst and landslides in Uttarakhand: A nature's fury. *Mausam*, **66**, 139–144.

Molinari, J., and D. Vollaro, 1989: External influences on hurricane intensity. Part I: Outflow layer eddy angular momentum fluxes. *J. Atmos. Sci.*, **46**, 1093–1105, https://doi.org/10.1175/1520-0469(1989)046<1093:EIOHIP>2.0.CO;2.

——, S. Skubis, and D. Vollaro, 1995: External influences on hurricane intensity. Part III: Potential vorticity structure. *J. Atmos. Sci.*, **52**, 3593–3606, https://doi.org/10.1175/1520-0469(1995)052<3593:EIOHIP>2.0.CO;2.

——, ——, ——, F. Alsheimer, and H. E. Willoughby, 1998: Potential vorticity analysis of tropical cyclone intensification. *J. Atmos. Sci.*, **55**, 2632–2644, https://doi.org/10.1175/1520-0469(1998)055<2632:PVAOTC>2.0.CO;2.

Montgomery, M. T., N. V. Sang, R. K. Smith, and J. Persing, 2009: Do tropical cyclones intensify by WISHE? *Quart. J. Roy. Meteor. Soc.*, **135**, 1697–1714, https://doi.org/10.1002/QJ.459.

Mooley, D. A., and J. Shukla, 1989: Main features of the westward-moving low pressure systems which form over the Indian region during the summer monsoon season and their relation to the monsoon rainfall. *Mausam*, **40**, 137–152.

Moorthi, S., and A. Arakawa, 1985: Baroclinic instability with cumulus heating. *J. Atmos. Sci.*, **42**, 2007–2031, https://doi.org/10.1175/1520-0469(1985)042<2007:BIWCH>2.0.CO;2.

Pai, D., L. Sridhar, M. R. Badwaik, and M. Rajeevan, 2015: Analysis of the daily rainfall events over India using a new long period (1901–2010) high resolution (0.25 × 0.25) gridded rainfall data set. *Climate Dyn.*, **45**, 755–776, https://doi.org/10.1007/S00382-014-2307-1.

Palazzi, E., J. Hardenberg, and A. Provenzale, 2013: Precipitation in the Hindu-Kush Karakoram Himalaya: Observations and future scenarios. *J. Geophys. Res. Atmos.*, **118**, 85–100, https://doi.org/10.1029/2012JD018697.

Patla, J. E., D. Stevens, and G. M. Barnes, 2009: A conceptual model for the influence of TUTT cells on tropical cyclone motion in the northwest Pacific Ocean. *Wea. Forecasting*, **24**, 1215–1235, https://doi.org/10.1175/2009WAF2222181.1.

Pfeffer, R. L., and M. Challa, 1981: A numerical study of the role of eddy fluxes of momentum in the development of Atlantic hurricanes. *J. Atmos. Sci.*, **38**, 2393–2398, https://doi.org/10.1175/1520-0469(1981)038<2393:ANSOTR>2.0.CO;2.

Pisharoty, P. R., and B. N. Desai, 1956: Western disturbances and Indian weather. *Indian J. Meteor. Geophys.*, **7**, 333–338.

Prasad, K., and D. Krishna Rao, 1974: Case studies of westerly waves in the development of monsoon depressions. *Indian J. Meteor. Geophys*, **25**, 265–268.

Rajamani, S., and K. V. Rao, 1981: On the occurrence of rainfall over southwest sector of monsoon depression. *Mausam*, **32**, 215–220.

Ramaswamy, C., 1976: Synoptic aspects of droughts in the Asiatic monsoon area. *Proc. Indian Natl. Sci. Acad.*, **42A**, 109–132.

Ranalkar, M. R., H. S. Chaudhari, A. Hazra, G. Sawaisarje, and S. Pokhrel, 2016: Dynamical features of incessant heavy rainfall event of June 2013 over Uttarakhand, India. *Nat. Hazards*, **80**, 1579–1601, https://doi.org/10.1007/s11069-015-2040-z.

Rao, B. R. S., D. V. B. Rao, and V. B. Rao, 2004: Decreasing trend in the strength of Tropical Easterly Jet during the Asian summer monsoon season and the number of tropical cyclonic systems over Bay of Bengal. *Geophys. Res. Lett.*, **31**, L14103, https://doi.org/10.1029/2004GL019817.

Rao, G. N., 2001: Occurrence of heavy rainfall around the confluence line in monsoon disturbances and its importance in causing floods. *J. Earth Syst. Sci.*, **110**, 87–94, https://doi.org/10.1007/BF02702232.

Rao, V. B., and S. T. Rao, 1971: A theoretical and synoptic study of western disturbances. *Pure Appl. Geophys.*, **90**, 193–208, https://doi.org/10.1007/BF00875523.

Rao, Y., 1976: *Southwest Monsoon*. Vol. 366. India Meteorological Department, 366 pp.

Rasul, G., Q.-U.-Z. Chaudhry, Z. Sixiong, Z. Qingcun, Q. Linlin, and Z. Gaoying, 2005: A diagnostic study of heavy rainfall in Karachi due to merging of a mesoscale low and a diffused tropical depression during South Asian summer monsoon. *Adv. Atmos. Sci.*, **22**, 375–391, https://doi.org/10.1007/BF02918751.

Rios-Berrios, R., R. D. Torn, and C. A. Davis, 2016: An ensemble approach to investigate tropical cyclone intensification in sheared environments. Part II: Ophelia (2011). *J. Atmos. Sci.*, **73**, 1555–1575, https://doi.org/10.1175/JAS-D-15-0245.1.

Rodgers, E. B., S. W. Chang, J. Stout, J. Steranka, and J.-J. Shi, 1991: Satellite observations of variations in tropical cyclone convection caused by upper-tropospheric troughs. *J. Appl. Meteor.*, **30**, 1163–1184, https://doi.org/10.1175/1520-0450(1991)030<1163:SOOVIT>2.0.CO;2.

Roy, S. S., and S. K. Roy Bhowmik, 2005: Analysis of thermodynamics of the atmosphere over northwest India during the passage of a western disturbance as revealed by model analysis field. *Curr. Sci.*, **88**, 947–951.

Sadler, J. C., 1976: A role of the tropical upper tropospheric trough in early season typhoon development. *Mon. Wea. Rev.*, **104**, 1266–1278, https://doi.org/10.1175/1520-0493(1976)104<1266:AROTTU>2.0.CO;2.

Saha, C. K., 2015: Dynamics of disaster-induced risk in southwestern coastal Bangladesh: An analysis on tropical cyclone Aila 2009. *Nat. Hazards*, **75**, 727–754, https://doi.org/10.1007/s11069-014-1343-9.

Schiemann, R., D. Lüthi, and C. Schär, 2009: Seasonality and interannual variability of the westerly jet in the Tibetan Plateau region. *J. Climate*, **22**, 2940–2957, https://doi.org/10.1175/2008JCLI2625.1.

Sen, S. N., 1959: Influence of upper level troughs and ridges on the formation of post monsoon cyclones in Bay of Bengal. *Indian J. Meteor. Geophys.*, **16**, 7–24.

Shi, J.-J., S. Wei-Jen Chang, and S. Raman, 1990: A numerical study of the outflow layer of tropical cyclones. *Mon. Wea.*

Rev., **118**, 2042–2055, https://doi.org/10.1175/1520-0493(1990)118<2042:ANSOTO>2.0.CO;2.

——, S. Chang, and S. Raman, 1997: Interaction between Hurricane Florence (1988) and an upper-tropospheric westerly trough. *J. Atmos. Sci.*, **54**, 1231–1247, https://doi.org/10.1175/1520-0469(1997)054<1231:IBHFAA>2.0.CO;2.

Sikka, D. R., 1977: Some aspects of the life history, structure and movement of monsoon depressions. *Pure Appl. Geophys.*, **115**, 1501–1529, https://doi.org/10.1007/BF00874421.

——, 2006a: Major advances in understanding and prediction of tropical cyclones over the North Indian Ocean: A perspective. *Mausam*, **57**, 165.

——, 2006b: A study on the monsoon low pressure systems over the Indian region and their relationship with drought and excess monsoon seasonal rainfall. Center for Ocean–Land–Atmosphere Studies Tech. Rep. 217, Center for the Application of Research on the Environment, 61 pp.

Singh, C., and R. Chand, 2015: Exceptionally heavy rainfall over Uttarakhand during 15-18 June, 2013—A case study. *Mausam*, **66**, 741–750.

Singh, M. S., and C. L. Agnihotri, 1977: Baroclinity over India in winter and its relation to western disturbances and jet streams. I. *Indian J. Meteor. Hydrol. Geophys.*, **28**, 303–310.

Singh, O. P., T. M. A. Khan, and M. S. Rahman, 2001: Has the frequency of intense tropical cyclones increased in the north Indian Ocean? *Curr. Sci.*, **80**, 575–580.

Srinivasan, V., K. Ramamurthy, and Y. R. Nene, 1973: *Summer—Nor'westers and Andhis and Large Scale Convective Activity over Peninsula and Central Parts of the Country*. India Meteorological Department, 137 pp.

Tomar, M. S., 2012: An insight into the severe floods in India during 2005, 2006 & 2007. *Mausam*, **63**, 65–70.

Vellore, R. K., and Coauthors, 2016: Monsoon-extratropical circulation interactions in Himalayan extreme rainfall. *Climate Dyn.*, **46**, 3517–3546, https://doi.org/10.1007/s00382-015-2784-x.

Webster, P. J., V. O. Magaña, T. N. Palmer, J. Shukla, R. A. Tomas, M. Yanai, and T. Yasunari, 1998: Monsoons: Processes, predictability, and the prospects for prediction. *J. Geophys. Res.*, **103**, 14 451–14 510, https://doi.org/10.1029/97JC02719.

Yasunari, T., 1986: Low-frequency interactions between the summer monsoon and the Northern Hemisphere westerlies. *J. Meteor. Soc. Japan*, **64**, 693–708, https://doi.org/10.2151/jmsj1965.64.5_693.

Yatagai, A., K. Kamiguchi, O. Arakawa, A. Hamada, N. Yasutomi, and A. Kitoh, 2012: APHRODITE: Constructing a long-term daily gridded precipitation dataset for Asia based on a dense network of rain gauges. *Bull. Amer. Meteor. Soc.*, **93**, 1401–1415, https://doi.org/10.1175/BAMS-D-11-00122.1.

——, N. Masuda, K. Tanaka, and A. Higuchi, 2017: APHRODITE-2: Improved grid precipitation algorithm—Initial results. *Abstr. Soc. Hydrol. Water Res.*, **30**, 30.

Zehr, R. M., 1992: Tropical cyclogenesis in the western North Pacific. Tech. Rep., NOAA Tech. Rep. NESDIS 61, 189 pp., https://repository.library.noaa.gov/view/noaa/13116/noaa_13116_DS1.pdf.